Northwest Africa 11024-A heated and dehydrated unique carbonaceous (CM) chondrite

Samuel Ebert, Addi Bischoff, Dennis Harries, Sarah Lentfort, Jean-Alix J-A Barrat, Andreas Pack, Jérôme Gattacceca, Robbin Visser, Peter Schmid-beurmann, Stephan Kimpel

The Meteoritical Society

Meteoritics & Planetary Science 54, Nr 2, 328–356 (2019)
doi: 10.1111/maps.13212

Northwest Africa 11024—A heated and dehydrated unique carbonaceous (CM) chondrite

Samuel EBERT[1*], Addi BISCHOFF[1], Dennis HARRIES[2], Sarah LENTFORT[1], Jean-Alix BARRAT[3], Andreas PACK[4], Jérôme GATTACCECA[5], Robbin VISSER[6], Peter SCHMID-BEURMANN[7], and Stephan KIMPEL[1]

[1]Institut für Planetologie, Westfälische Wilhelms-Universität Münster, Wilhelm-Klemm-Str. 10, D-48149 Münster, Germany
[2]Institut für Geowissenschaften, Friedrich-Schiller-Universität Jena, Carl-Zeiss-Promenade 10, D-07745 Jena, Germany
[3]Institut Universitaire Européen de la Mer, Université de Bretagne Occidentale, Place Nicolas Copernic, F-29280 Plouzané Cedex, France
[4]Geowissenschaftliches Zentrum, Universität Göttingen, Goldschmidtstr. 1, D-37077 Göttingen, Germany
[5]CNRS, Aix Marseille Université, IRD, INRA, College de France, CEREGE, Aix-en-Provence, France
[6]Institut für Geologische Wissenschaften, Freie Universität Berlin, Malteserstr. 74-100, D-12249 Berlin, Germany
[7]Institut für Mineralogie, Westfälische Wilhelms-Universität Münster, Corrensstraße 24, D-48149 Münster, Germany
[*]Corresponding author. E-mail: samuel.ebert@uni-muenster.de

(Received 07 March 2018; revision accepted 08 October 2018)

Abstract–Based on the high abundance of fine-grained material and its dark appearance, NWA 11024 was recognized as a CM chondrite, which is also confirmed by oxygen isotope measurements. But contrary to known CM chondrites, the typical phases indicating aqueous alteration (e.g., phyllosilicates, carbonates) are missing. Using multiple analytical techniques, this study reveals the differences and similarities to known CM chondrites and will discuss the possibility that NWA 11024 is the first type 3 CM chondrite. During the investigation, two texturally apparent tochilinite–cronstedtite intergrowths were identified within two thin sections. However, the former phyllosilicates were recrystallized to Fe-rich olivine during a heating event without changing the textural appearance. A peak temperature of 400–600 °C is estimated, which is not high enough to destroy or recrystallize calcite grains. Thus, calcites were never constituents of the mineral paragenesis. Another remarkable feature of NWA 11024 is the occurrence of unknown clot-like inclusions (UCLIs) within fine-grained rims, which are unique in this clarity. Their density and S concentration are significantly higher than of the surrounding fine-grained rim and UCLIs can be seen as primary objects that were not formed by secondary alteration processes inside the rims. Similarities to chondritic and cometary interplanetary dust particles suggest an ice-rich first-generation planetesimal for their origin. In the earliest evolution, NWA 11024 experienced the lowest degree of aqueous alteration of all known CM chondrites and subsequently, a heating event dehydrated the sample. We suggest to classify the meteorite NWA 11024 as the first type 3 CM chondrite similar to the classification of CV3 chondrites (like Allende) that could also have lost their matrix phyllosilicates by thermal dehydration.

INTRODUCTION

Chondritic meteorites mainly consist of four major components: chondrules, Fe,Ni metal/troilite, refractory inclusions, and fine-grained material (fine-grained dust rims [FGRs] and matrix). CI chondrites are the only exception. They are complex breccias and their primary mineralogy was almost entirely obliterated by aqueous alteration on their parent body(ies) at temperatures of ~50–150 °C (e.g., Richardson 1978; McSween 1979a; Zolensky et al. 1989a; Endreß and Bischoff 1996; Endress et al. 1996; Brearley 2006; Morlok et al. 2006). However,

despite strong modifications by impact processes and nearly complete alteration by water, they are regarded as the most primitive meteorites and provide the best chemical match compared to that of the solar photosphere (e.g., Anders and Grevesse 1989; Palme and Jones 2003; Lodders et al. 2009; Barrat et al. 2012).

The importance of water in the early evolution of asteroids is also illustrated by the fact that water did not only alter CI chondrites but also other chondrites like CM, CR, CV, CO, and ordinary chondrites (e.g., Zolensky et al. 1999; Brearley 2006; Dyl et al. 2012). Although metamorphosed chondrites are basically regarded as dry meteorites, Zolensky et al. (1999) and Dyl et al. (2012) showed that even the metamorphosed ordinary chondrites Monahans (H5) and Villalbeto de la Pena (L6) are affected by asteroidal water. Furthermore, spectral investigations of type B, C, F, and G asteroids revealed that hydrous phyllosilicates are possibly present at their surface, similar to those of CI and CM chondrites (e.g., Vilas and Gaffey 1989; Gaffey et al. 1993; Kanno et al. 2003; Rivkin et al. 2015; Vernazza et al. 2016). Water is certainly widespread in the solar system and not a negligible component during meteorite parent body formation and is playing a key role in the understanding of the early solar system processes.

Different sources of water in meteorite parent bodies are possible to explain the occurrence of phyllosilicates and phases formed from aqueous fluids (e.g., carbonates, phosphates, magnetites). It could result from molten ice that has been accreted in the parent body (e.g., Grimm and McSween 1989) and/or water-bearing phyllosilicates may be formed directly in the solar nebula (Petaev and Wood 1998; Ciesla et al. 2003; Wasson and Trigo-Rodríguez 2004; Ciesla and Lauretta 2005). The incorporated water starts to react with the surrounding material (silicates, metals, sulfides) at low temperatures. Different heat sources like the decay of ^{26}Al (McSween et al. 1988), short local heating events caused by impacts, or solar radiation (Nakato et al. 2008) result in low aqueous alteration temperatures of 0–150 °C for CI and CM chondrites (e.g., Richardson 1978; McSween 1979a; Clayton and Mayeda 1984, 1999; Zolensky and McSween 1988; Zolensky et al. 1989a, 1993; Endreß and Bischoff 1996; Endress et al. 1996; Verdier-Paoletti et al. 2017).

Besides the CI chondrites, CM chondrites experienced the strongest modifications by aqueous alteration resulting in different water-bearing phases. These new minerals either formed by reaction of the fluid with primary anhydrous phases (e.g., Fe-Mg serpentines, cronstedtite, and tochilinite) or as direct precipitates from fluids (e.g., carbonates or fine-grained serpentines). Carbonates in particular are a minor but ubiquitous constituent in CM chondrites, as grains and veins, and are even present in the least altered meteorites like Maribo (Haack et al. 2012), Paris (Hewins et al. 2014; Marrocci et al. 2014; Rubin 2015), and Elephant Moraine (EET) 96029 (Lee et al. 2016). However, the physics, chemistry, location, timing, and duration of the processes of aqueous alteration are still poorly understood (e.g., Metzler et al. 1992; Metzler 1995; Metzler and Bischoff 1996; Bischoff 1998; Bischoff et al. 2006; Brearley 2006).

The aqueous alteration could have taken place as postaccretionary in situ alteration after the formation of the CM parent body (e.g., Kerridge and Bunch 1979; Zolensky and McSween 1988; Browning et al. 1996; Trigo-Rodríguez et al. 2006; Rubin et al. 2007), directly in the solar nebula (Grossman and Larimer 1974; Ciesla et al. 2003), or in loosely consolidated first-generation planetesimals (Metzler et al. 1992; Metzler and Bischoff 1996; Bischoff 1998; Metzler 2004; Lindgren et al. 2013). However, the lifetime of the solar nebula is poorly constrained and dating of secondary minerals (like calcite) alone cannot distinguish between nebular and asteroidal settings (Podosek and Cassen 1994; Krot et al. 2006). The aqueous alteration could have started contemporaneous with or shortly after CAI formation and lasted at least 4 Ma (e.g., De Leuw et al. 2009) or alternatively, the alteration took place at a late stage (>3 Ma) after the formation of differentiated and metamorphosed asteroids (Fujiya et al. 2012). But, investigations on the paleomagnetism have shown that the magnetic solar nebula field and therefore the nebular gas too, had dispersed until ~4–6 Ma after CAIs (Gattacceca et al. 2016; Wang et al. 2017). This is also the time scale for planet migration and the accretion of ice and water-bearing minerals.

The water is mainly bound in phyllosilicates (e.g., Tomeoka and Buseck 1985) and typical CM chondrites contain ~6–14 wt% water (Jarosewich 1990; Alexander et al. 2012, 2013; Garenne et al. 2014). The incorporated water starts to react with the surrounding material and different classification schemes have been proposed to quantify the degree of alteration in CM chondrites (Browning et al. 1996; Rubin et al. 2007; Howard et al. 2009; Alexander et al. 2012, 2013). For example, in the classification scheme of Rubin et al. (2007), the FeO/SiO_2 ratio of serpentine–tochilinite intergrowths (formerly called PCP—poorly/partly characterized phases), the amount and size of serpentine–tochilinite intergrowths and the abundances of metals and Ca-carbonates are important to define the CM2 subtypes. Howard et al. (2009) and Alexander et al. (2012, 2013) quantified the extent of aqueous alteration based on the abundance of phyllosilicates, which roughly correlates with the classification of Rubin et al. (2007). However, most CM chondrites are impact breccias and different clasts of

variable sizes show different degrees of alteration (Fuchs et al. 1973; Dodd 1981; Rubin and Wasson 1986; Metzler et al. 1992; Metzler 1995; Bischoff 1998; Bischoff et al. 2006, 2017a). Rubin et al. (2007) considered this aspect and used the main lithology of a thin section to define the subtype of the CM2 sample. However, the main lithology can vary from sample to sample of one particular meteorite as shown for Nogoya (Bischoff et al. 2017a). Because of this aspect, Bischoff et al. (2017a) proposed an extended description of the sample (e.g., CM 2.2–2.5) in the same way as for ordinary chondrite breccias, to avoid an "average" value for the degree of alteration. This type of classification would take into account (1) the brecciation of the meteorite as well as (2) the degree of alteration of the different fragments.

We have a systematic classification scheme for thermally metamorphosed chondrites (petrologic types 3–6; Van Schmus and Wood 1967) and aqueously altered chondrites (petrologic types 1–2; Van Schmus and Wood 1967). Considering the sample discussed in this work, these schemes are not applicable for meteorites, which acquired aqueous alteration and subsequently lost their water by thermal processes.

However, heated (thermally metamorphosed) carbonaceous chondrites exist in a non-negligible abundance and have been studied in detail. The best-known heated carbonaceous chondrites are the members of the so-called Belgica grouplet encompassing Y-82162, Y-86720, and B-7904 (e.g., Mayeda et al. 1987; Akai 1988, 1989, 1990a, 1990b, 1992; Tomeoka 1989; Zolensky et al. 1989b; Mayeda and Clayton 1990; Paul and Lipschutz 1990; Bischoff and Metzler 1991; Ikeda 1992), but many other samples are known (e.g., Y-793321 [Akai 1990a; Nakamura 2005, 2006; Harries and Langenhorst 2013]; Y-86029 [Tonui et al. 2002, 2003]; and A-881334, Y-82098, and Y-86695 [Akai and Tari 1997]). Heating processes are responsible for the dehydration of phyllosilicates (Akai 1988, 1990a; Tomeoka et al. 1989; Zolensky et al. 1989a) and recrystallization resulting in secondary formation of e.g., olivine and pyroxene (Akai 1990a, 1992; Zolensky et al. 1993; Nakamura 2005). C-type asteroids with similar mineralogical characteristics exist that may indicate formation of a dry asteroid surface caused by heating and dehydration (Hiroi et al. 1993, 1994, 1996; Hiroi and Zolensky 1999).

The estimated temperature ranges are 300–500 °C for Y-93321 (Akai 1990a; Nakamura 2005, 2006; Harries and Langenhorst 2013) and 500–600 °C for Y-86029 (Tonui et al. 2003). Higher temperatures are estimated for the Belgica grouplet (500–900 °C; Tomeoka et al. 1989; Akai 1990a, 1992; Paul and Lipschutz 1990; Zolensky et al. 1991, 1993; Lipschutz et al. 1999; Tonui et al. 2002; Nakamura 2005, 2006; Nakato et al. 2008).

In these temperature ranges, heating processes decompose Fe,Ni sulfides creating Ni-poor metals (Kimura et al. 2011; Harries and Langenhorst 2013). Kimura et al. (2011) subdivided heated carbonaceous chondrites into category A, B, and C depending on their experience of secondary thermal processing in opaque minerals (e.g., Fe,Ni sulfides). Furthermore, Nakamura (2005) defined four different heating stages (I–IV) based on diverse stages of reaction recognized in serpentine and saponite (Akai 1992). The question is still open as to how we handle the classic classification scheme with the heating stages, because heating processes can destroy aqueous alteration products and characteristics and a typical subclassification (CM2, CV3, or CI2) is no longer possible.

All the abovementioned aspects may trigger discussion on a possible expansion of the current classification scheme. The meteorite NWA 11024, the focus of this study, is a new heated CM chondrite that does not fit into this scheme. The sample lacks water, phyllosilicates, and even calcite grains. Furthermore, the sample differs from other CM chondrites by the presence of abundant, so-far unknown clot-like inclusions (UCLIs) within the fine-grained rims (FGRs) which are unique in this clarity. In this work, the mineralogical and chemical characteristics of this new meteorite are presented including data of oxygen isotopic analysis, X-ray diffraction, Raman spectroscopy, magnetic properties, and TEM investigations in order to decipher the basic processes of formation and evolution of this rock.

SAMPLE AND METHODS

The meteorite NWA 11024 (4.69 g; Fig. 1) was purchased in Ensisheim from a Moroccan dealer in June 2014. Two polished thin sections, PL17074 (thin section A; Fig. 2) and PL17073 (thin section B), were prepared for further investigations.

Optical and Electron Microscopy

The thin sections (A and B) from NWA 11024 were studied by optical and electron microscopy. For optical microscopy in transmitted and reflected light, a ZEISS polarizing microscope (AXIOPHOT) was used.

A JEOL 6610-LV electron microscope at the Interdisciplinary Center for Electron Microscopy and Microanalysis (ICEM) at the Westfälische Wilhelms-Universität Münster was used to study the fine-grained textures of NWA 11024, its components, and to identify the different mineral phases.

The secondary electron microscope (SEM) was also used for quantitative analysis. Samples and

Fig. 1. The bulk sample of NWA 11024 weighing 4.69 g. (Color figure can be viewed at wileyonlinelibrary.com.)

appropriate mineral standards were measured at an excitation voltage of 20 kV and the beam current constancy was controlled by a Faraday cup. With the attached EDS system, a bulk chemical characterization of thin section A was performed and analyses of the different mineral constituents were obtained. As natural and synthetic standards from Astimex, olivine (Mg, Fe, Si), jadeite (Na), plagioclase (Al), sanidine (K), diopside (Ca), rutile (Ti), chromium oxide (Cr), rhodonite (Mn), and pentlandite (Ni) were used as standards for mineral analyses. The EDS analyses were done with the INCA analytical program provided by Oxford Instrument.

Electron Microprobe Analysis

Quantitative mineral analyses and matrix analyses were obtained using a JEOL JXA 8900 Superprobe electron microprobe at the ICEM, which was operated at 15 kV and a probe current of 15 nA. Natural and synthetic standards were used for wavelength dispersive spectrometry. Jadeite (Na), kyanite (Al), sanidine (K), chromium oxide (Cr), San Carlos olivine (Mg), hypersthene (Si), diopside (Ca), rhodonite (Mn), rutile (Ti), fayalite (Fe), apatite (P), celestine (S), and nickel oxide (Ni) were used as standards for bulk and mineral analyses. The measurement time was 7.5 s for Na and K and 15 s for the other elements. The mineral analyses were conducted with variable spot sizes between up to 10 μm and the matrix analyses with a constant spot size of 15 μm. The mean detection limits for the microprobe were ~0.02–0.08 wt%. The matrix corrections were made according to the Φρ(z) procedure (Armstrong 1991).

Image Analysis

Image analyses were performed with the software JMicrovision (www.jmicrovision.com). The modal abundances of the different phases and components were determined by point counting (4000 points on each thin section) of backscattered electron (BSE) mosaic images.

Oxygen Isotope Analysis

The oxygen isotope composition of NWA 11024 was analyzed by means of laser fluorination in combination with gas source mass spectrometry (Sharp 1990) at the Department of Isotope Geology, University Göttingen. Two aliquots were analyzed. The samples were loaded along with San Carlos olivine in a 19-pit stainless steel sample holder. We used a two-window (quartz glass viewing port and BaF_2 for the CO_2 laser beam) sample chamber as described in Sharp (1990). The samples were fluorinated with ~40 mbar BrF_5. The unwanted gaseous reaction products (mainly BrF_5-x and SiF_4) were removed by means of cryogenic trapping. The sample O_2 was collected at −196 °C on 5 Å molecular sieve for 7 min. For further purification (removal of N_2 and NF_3), sample O_2 was transported with a He carrier gas stream through a 3 m long packed molecular sieve gas chromatography column (Restek) that was kept at 50 °C. The sample O_2 was then collected downstream in a second, low-volume molecular sieve trap. After evacuation of He from the second trap, sample O_2 was expanded to the bellows of a Thermo MAT253 gas source mass spectrometer. The sample gas was analyzed relative to a working gas for ~30 min (20 cycles). The external reproducibility of San Carlos olivine measurements was 0.1‰ for $\delta^{18}O$ and 0.008‰ for $\Delta'^{17}O$ (1σ SD, single analysis). The data were normalized to the composition of San Carlos olivine ($\delta^{17}O_{VSMOW2}$ = 2.715, $\delta^{18}O_{VSMOW2}$ = 5.220‰; see Pack et al. 2016).

Bulk Chemical Analysis

A 500 mg whole-rock sample was homogenized and dissolved following the procedure described by Barrat et al. (2012, 2016). No residual grains were observed in the solution. The concentrations of Ti, Al, Cr, Fe, Mn, Mg, Ca, Na, P, Co, and Ni were determined by ICP-AES (inductively coupled plasma-atomic emission spectrometry) using a Horiba Jobin Yvon Ultima 2

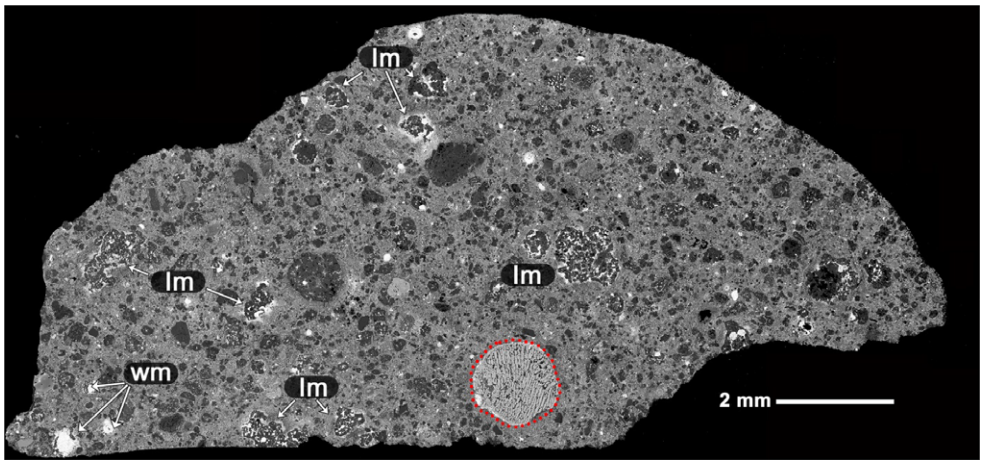

Fig. 2. Photomicrograph of a representative part of NWA 11024 (thin section A). Large chondrules of different composition (type I, type Im, and type II) are clearly visible as well as abundant fine-grained material. Besides the type Im chondrules, the large type II chondrule (red dotted line) is an eye catcher. Image in backscattered electrons (BSE). Im = type Im chondrules; wm = weathered metal. (Color figure can be viewed at wileyonlinelibrary.com.)

spectrometer following the procedure of Cotten et al. (1995). The concentrations of trace elements were determined by ICP-SFMS (inductively coupled plasma-sector field mass spectrometry) using a Thermo Element 2 spectrometer following the procedures described by Barrat et al. (2007, 2008).

Raman Spectroscopy

Raman spectra were acquired with a Horiba ISA Dilor Labram micro confocal Raman spectrometer with a focal length of 300 mm and equipped with an external 532.15 nm Nd-YAG laser at the Freie Universität Berlin. The laser power on the surface of the samples was of 2–3 mW and did not show any signs of heating or alteration of the carbonaceous material. Spectra were corrected for drift using a 520.7 cm^{-1} silica standard and the obtained full widths at half maximum (FWHM) were corrected for the spectral resolution of the Raman according to the apparatus function by Irmer (1985).

The acquisition time for one spectrum was 30 s with a spot size of 1 μm. All spectra were decomposed using four pseudovoigt functions (Homma et al. 2015). A high coefficient of determination ($R^2 > 0.99$) excluded a large portion of inaccurate fits, after which undetected anomalies were excluded manually resulting in a total of 124 spectra throughout the whole sample.

These measurements can be seen as a Raman carbon thermometer which is based on the irreversible change of organic material structure with increasing temperature. The sensitivity of Raman spectrometry, to the vibration in the bonds between atoms, detects these morphological changes in spectra and was first correlated to peak temperatures by Beyssac et al. (2002). Homma et al. (2015) modified the detailed Kouketsu et al. (2014) carbon geothermometer for the use on meteorites. The correlation shown in Equation 1 uses the D1-band (see Fig. 13a) of analyzed spectra to estimate the peak temperature of NWA 11024 (Homma et al. 2015).

$$T_{\text{peak}}{}^{\circ}\text{C} = -6.9 \times \text{FWHM}_{D1} + 1054.4 \quad (1)$$

X-Ray Diffraction

For qualitative phases, analysis of bulk material and characterization of NWA 11024 X-ray diffraction (PXRD) patterns were recorded using a Philips X'Pert PW 3040 powder diffractometer with monochromatic Cu-Kα1 radiation of λ = 1.5406 Å at the Institut für Mineralogie (University of Münster). The measurements were performed at 45 kV and 40 mA and room temperature over an angular range (2Θ) of 4.995° to 21.991° with a step size of 0.014° resulting in 1214 measurement points. Qualitative phase analysis was performed using the "Highscore" software of PANalytical B.V. Since there is only a very small amount of material from sample NWA 11024 left, X-ray diffraction measurements were made on a piece of the sample and not on a powdered sample.

Magnetic Properties

Hysteresis properties and magnetic susceptibility were measured on two thin sections and a 933 mg bulk sample at CEREGE (Aix-en-Provence) using a

Table 1. Modal abundances of constituents in NWA 11024 compared to the mean abundances of similar components within NWA 5958 (Jacquet et al. 2016). Data in vol%.

Sample	Type I	Type II	Matrix	FGR	Metals	Sulfides	CAIs	Clasts
NWA 11024 - A	30.1	3.2	50.9	10.6	2.3[a]	0.5	1.4	1.0
NWA 11024 - B	28.8	1.4	56.0	9.0	2.6[a]	0.4	1.1	0.7
NWA 5958	16.6	2.3	75.5[c]		3.6[b]		0.6	

[a]Includes Fe,Ni metals as well as alteration products of metal/sulfides.
[b]Includes all opaque phases (FeS, metal, and terrestrial, metal-sulfide-related weathering products).
[c]Including matrix material and fine-grained rims.

Princeton Micromag vibrating sample magnetometer (noise level 10^{-8} Am^2) and a MFK susceptibility meter (noise level 10^{-11} m^3), respectively. Mass-normalized parameters, such as saturation magnetization (a proxy to the total bulk amount of magnetic minerals), were obtained only from the bulk sample because the mass of the rock in the thin sections could not be determined precisely.

Transmission Electron Microscopy

At the University of Jena two samples were extracted for transmission electron microscopy (TEM) using focused ion beam (FIB) preparation (Harries and Langenhorst 2013). The FIB samples were studied using a 200 keV FEI Technai G2 equipped with an Oxford SDD EDS detector and a Fischione HAADF detector for scanning TEM imaging. EDS data of silicates were quantified using the Cliff–Lorimer method with electroneutrality-based thickness constraints for the absorption correction (Van Cappellen and Doukhan 1994). Analyses of metal grains were corrected for absorption using a thickness estimated from SEM images obtained during sample preparation. The k factors for the Cliff–Lorimer quantification were measured on standard samples (pallasite olivine and synthetic Fe,Ni alloy) or estimated based on standard measurements and factory-provided values in the INCA software.

RESULTS

Mineralogy and Petrography

General Description

Two thin sections were prepared from the sample and used for further investigations. Preliminary data were published by Ebert et al. (2017a). Thin section A (Fig. 2) has an area of ~80 mm² and consists of 50.9 vol% matrix, 10.6 vol% fine-grained dust rims (FGRs), 30.1 vol% type I chondrules, and 3.2 vol% type II chondrules (Table 1). Furthermore, 1.4 vol% CAIs and other minor components including metals, sulfides, and different clasts (Fig. 3) were identified. The irregularly shaped, forsterite- and enstatite-rich objects typically containing high abundances of opaque phases (Fig. 4) were also counted as type I chondrules. McSween (1977) described this type of objects in CV and CO chondrites as "similar to type I chondrules with addition of disseminated opaque grains," but usually those are "larger and more irregularly shaped than type I chondrules." In the following, they will be called type Im chondrules (type Im = irregularly shaped metal-rich type I chondrules).

Thin section B has an area of ~55 mm² and consists of 56 vol% matrix, 9.0 vol% of fine-grained dust rims, 29 vol% of type I chondrules, 1.5 vol% of type II chondrules, and 1.1 vol% of CAIs (Table 1). The differences in the abundance of type II chondrules between thin section A and B is caused by a huge type II chondrule in thin section A (Fig. 2). Modal abundances of the CM chondrites are highly variable, but NWA 11024 is in agreement with other CM chondrites (e.g., Metzler et al. 1992; Hewins et al. 2014; Jacquet et al. 2016). For example, the abundances of type I chondrules in NWA 11024 is higher than in NWA 5958, but lower than in Paris (Table 1).

NWA 11024 is dominated by fine-grained material (matrix and FGRs). Considering chemical analyses, it is suggested that this material mainly consists of a mixture of olivine and pyroxene grains often too small to be measured separately. Some measurable olivine and pyroxene grains reveal $Fo_{99–64}$ and $Fs_{2.8–12.5}$, respectively (Table S1 in supporting information).

The matrix mineralogy suffered from a strong terrestrial weathering, which is visible by a schlieren-like appearance and nearly all of the Fe,Ni metals are weathered but still dominant and clearly visible (Fig. 2). Electron microprobe measurements of the matrix show a mean total of ~93 wt% (Table 2). This is distinctly higher than the mean value of CM chondrites matrices (~79 wt%; e.g., McSween and Richardson 1977). All singe matrix measurements are listed in the supporting information (Table S2).

Calcite grains or large serpentine–tochilinite intergrowths (TCIs) are absent in the matrix which are

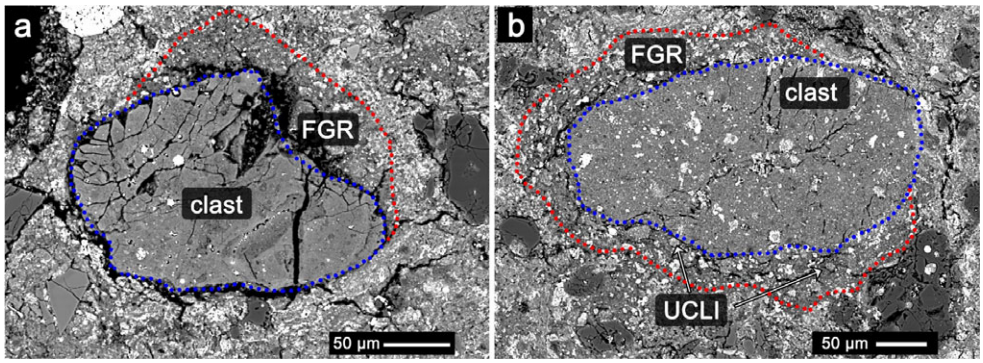

Fig. 3. Backscattered electron images of two foreign clast in the matrix of NWA 11024. Both are partly surrounded by a fine-grained rim. a) The fine-grained rim (red dotted line) partly surrounding the clast (blue dotted line). The gray ground-mass is pervaded by cracks. b) The clast (blue dotted line) is nearly completely surrounded by a fine-grained rim (red dotted line) and UCLIs are present. (Color figure can be viewed at wileyonlinelibrary.com.)

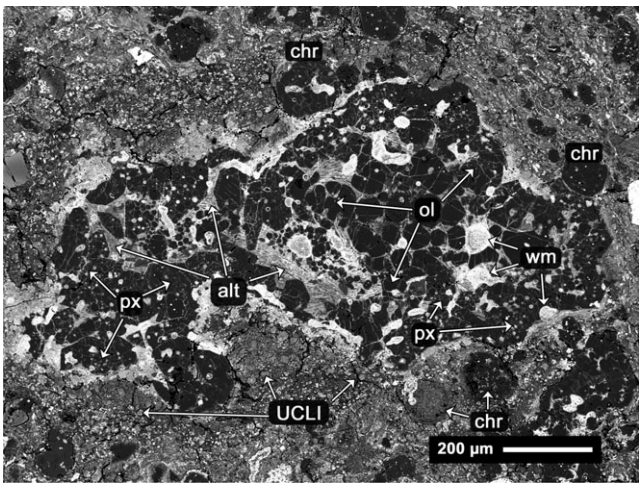

Fig. 4. Backscattered electron image of a type Im chondrule. The metal-bearing and porphyritic chondrules are a prominent part of NWA 11024. They are surrounded by a fine-grained dust rim with unknown clot-like inclusions (UCLIs; arrows). Olivine, pyroxene, weathered metals, and altered mesostasis are the prominent phases. Some olivines contain small Ni-poor metal grains. Some other small rounded chondrules (chr) are sticking onto the bigger type Im chondrule also embedded within the fine-grained dust rim. UCLI = unknown clot-like inclusion; px = pyroxene; ol = olivine; alt = altered mesostasis; wm = weathered metals; chr = chondrules.

normally present in all CM chondrites even in the low-altered CM chondrites like Paris (Hewins et al. 2014; Marrocci et al. 2014; Rubin 2015) or Maribo (Haack et al. 2012). Some single patches (<5 µm) in the matrix have been found (see Fig. 8c) that look like phyllosilicates. However, SEM and microprobe investigations show that these patches have totals of 92–99 wt% ruling out the occurrence of abundant water which is typical for phyllosilicates in CM2 chondrites.

Table 2. Mean concentrations of matrix, fine-grained rims (FGR), and unknown clot-like inclusions (UCLIs). All single measurements are in the supporting information Tables S2, S3, and S4.

	Matrix	FGR	UCLIs
n	72	106	83
Na_2O	0.34	0.40	0.27
MgO	14.1	15.9	14.7
Al_2O_3	2.67	2.36	2.28
SiO_2	25.0	27.0	25.1
P_2O_5	0.52	0.30	0.21
SO_3	9.8	4.8	9.3
Cl	0.15	0.20	0.15
K_2O	0.20	0.24	0.18
CaO	1.45	1.11	0.65
TiO_2	0.06	0.07	0.06
FeO	36.3	30.6	39.7
CoO	0.11	0.16	0.15
Cr_2O_3	0.31	0.54	0.36
MnO	0.27	0.28	0.26
NiO	1.59	2.55	1.83
Total	92.9	86.5	95.3

n = number of measurements; all data in wt%.

Chondrules and Chondrule Fragments

About 30 vol% of the thin sections are chondrules or chondrule fragments showing different textures (e.g., porphyritic and nonporphyritic) and compositions (type I, Im, and II). Most chondrule olivines have $Fa_{<4}$, and also olivines with higher Fa-content (up to Fa_{63}) exist (Fig. 5). Similarly, most low-Ca pyroxenes are enstatites ($Fs_{<2}$), and also some low-Ca pyroxenes with somewhat higher Fs-contents exist (e.g., $Fs_{5–13}$) as well as a compound chondrule (Fig. 6c). This complex chondrule consists of at least three siblings (compare e.g., Wasson et al. [1995] and Bischoff et al. [2017b]) and contains abundant Fe-rich olivine ($Fa_{52–63}$) and low-Ca pyroxene

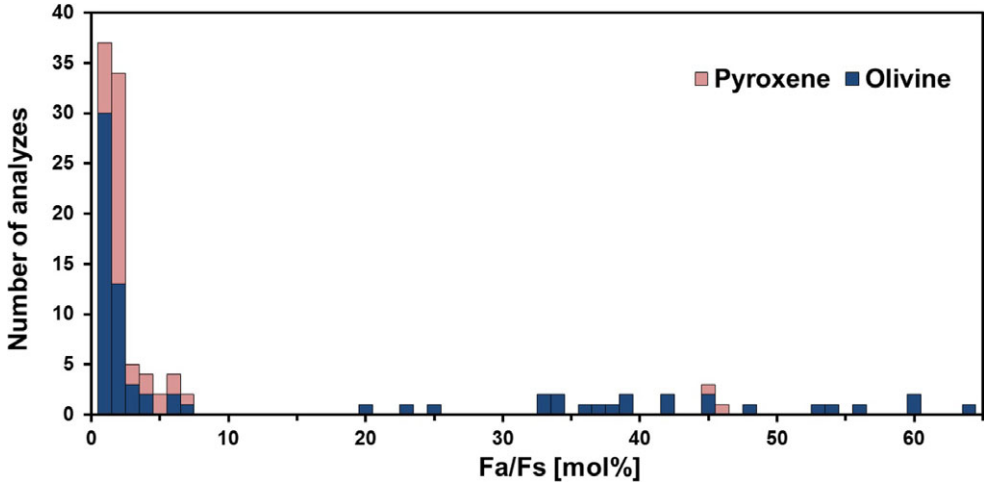

Fig. 5. Distribution of Fa and Fs contents in olivine (n = 74) and low-Ca pyroxene (n = 40), respectively. (Color figure can be viewed at wileyonlinelibrary.com.)

(~Fs_{45}). The remaining largely unweathered metal grains are Ni-poor (~6 wt% Ni; kamacite), but small metal grains in chondrules (mainly enclosed in Fo-rich olivines) can be Ni-rich (>50 wt% Ni). Al-rich chondrules as described by Bischoff and Keil (1983, 1984), Ebert and Bischoff (2015, 2016), and Ebert et al. (2017b, 2018) were not encountered.

Most of the chondrules are between 150 and 300 μm in apparent diameter, but individual chondrules can be as large as 1500 μm (Figs. 2 and 6a). Microchondrules of sizes <50 μm are present in the matrix, similar in size to those described by Krot et al. (1997a). Most of the chondrules and microchondrules are well-rounded, whereas some others are not (Fig 6d). Especially, type Im chondrules (Figs. 2 and 3) show irregular shapes, but have internal textures indicating crystallization of olivine from a melt (olivines are embedded within altered mesostasis materials). The mesostasis inside the chondrules—replaced by secondary phases—optically appears to consist of phyllosilicates, but SEM and microprobe measurements reveal totals between 94 and 98 wt%. Similar totals of 92–96 wt% were obtained from different areas of the conspicuous chondrule shown in Fig. 6b.

Ca,Al-Rich Inclusions

A total number of 82 Ca,Al-rich inclusions (CAIs) have been found and studied in both thin sections resulting in a modal abundance of ~1.3 vol%. Most CAIs are small (<100 μm; the smallest has an apparent size of 15 μm and the largest has a size of 490 μm). Some CAIs are enclosed or partly surrounded by a fine-grained dust rim (Fig. 7).

The compositions of various selected mineral phases in different CAIs from NWA 11024 are listed in Table 3. The most common phases are spinel, different Ca-pyroxenes ($Fs_{0.4–5.2}$) like diopside, Al-diopside, fassaite, and olivine ($Fo_{96.6–99.7}$). Most of the olivine occurs as a rim around a spinel- and Ca-pyroxene-rich core (Figs. 7a and 7b), but could also be found as small inclusions inside the CAI. Rare phases are perovskite and hibonite, whereas melilite is not present within the CAIs of both thin sections. One CAI contains a Ca-phosphate-rich phase (perhaps merrillite), but could not be definitely identified because of its small size. Another CAI includes a small PGE-nugget (Fig. 7b) with minor perovskite grains surrounded by spinel, Al-diopside, and a small rim of olivine. Furthermore, most inclusions show secondary phases like sulfides and alteration products (Figs. 7c and 7e). Most CAIs belong to the fine-grained, "fluffy," spinel- and pyroxene-rich inclusions and the others are "simple" CAIs. Six fine-grained aggregates exist, which are not clearly confined to the surrounding matrix material and could only be identified as CAIs through Ca,Al-rich phases by Ca- and Al-X-ray maps. The "fluffy" CAIs often show a contorted/sinuous morphology (Figs. 7a, 7b, 7e, and 7f) and many are fragmented (Fig. 7c), while the "simple" CAIs (Fig. 7d) typically have a simple core–rim structure with a spinel core and a diopside rim. All single measurements of the different phases are listed in the appendix (Table S5 in supporting information).

Phyllosilicate Pseudomorphs

Additional to the former phyllosilicates (<5 μm) in the matrix, two larger fibrous aggregates texturally similar to TCIs (tochilinite–cronstedtite intergrowths) are present (Fig. 8). The phyllosilicate pseudomorph TCI-1 consists of several large objects (each ~50 μm) surrounding a fragmented CAI (Fig 8a). The different

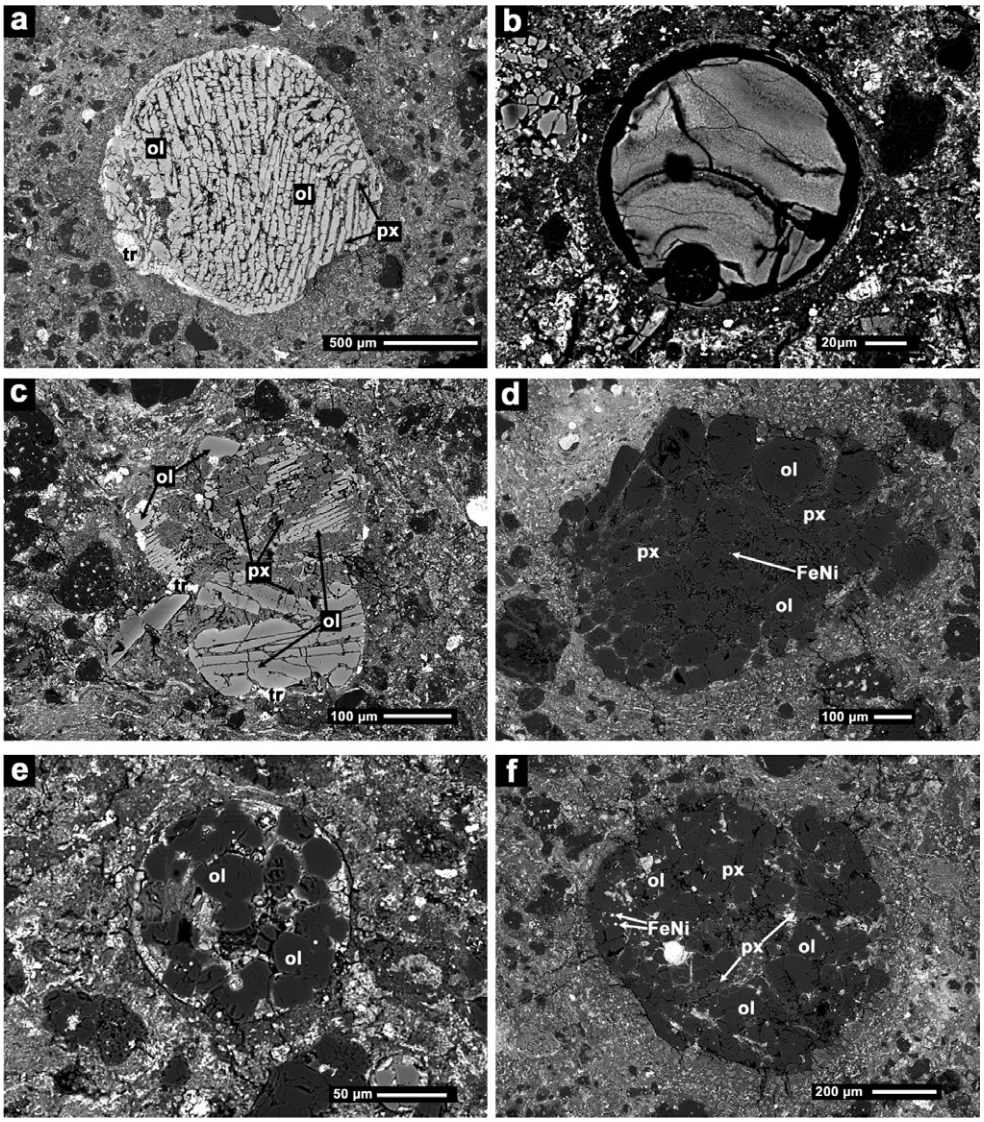

Fig. 6. Backscattered electron images of six different chondrules. a) Type II, barred-olivine chondrule surrounded by a FGR. The interior mesostasis was altered to secondary phase. Troilite and Fe,Ni metal with high Ni content are present. b) Texturally unusual chondrule with a huge space between the interior and the fine-grained rim. c) Complex compound chondrule consisting of three chondrules mainly made of olivines and pyroxenes and partly surrounded by FGR. d) Porphyritic olivine pyroxene (POP) chondrule partly surrounded by a FGR. The interior mesostasis is replaced by secondary alteration products, but small grains of Fe,Ni grains (arrow) are still present. e) Porphyritic olivine chondrule with clearly visible altered mesostasis. f) POP type I chondrule with minor Fe,Ni metal grains; Ol = olivine, px = pyroxene; FeNi = Fe,Ni metal.

patches have different shades of gray in the backscatter electron (BSE) images. Two brighter patches show a black rim (perhaps porous material), whereas the other patches are somewhat darker and do not have that prominent black rim. The totals vary in the different clasts from 92 to 97 wt%. A FIB section (more in the TEM investigations section) was made from one TCI-looking patch (red line, Fig. 8a).

The phyllosilicate pseudomorph TCI-2 (Fig. 8b) is a single TCI-looking patch with totals up to 96 wt%. The interior is dominated by a fibrous texture. TCI-2 is partly surrounded by a FGR and an AOA (amoeboid olivine aggregate) is directly connected to the TCI-patch. Small cracks around the TCI-2 are present but not as prominent as for TCI-1.

Unknown Clot-Like Inclusions

A remarkable feature in the sample NWA 11024 is the unknown clot-like inclusions (UCLIs; Figs. 4, 6d, 7e, 7f, and 9). These small objects are widespread within

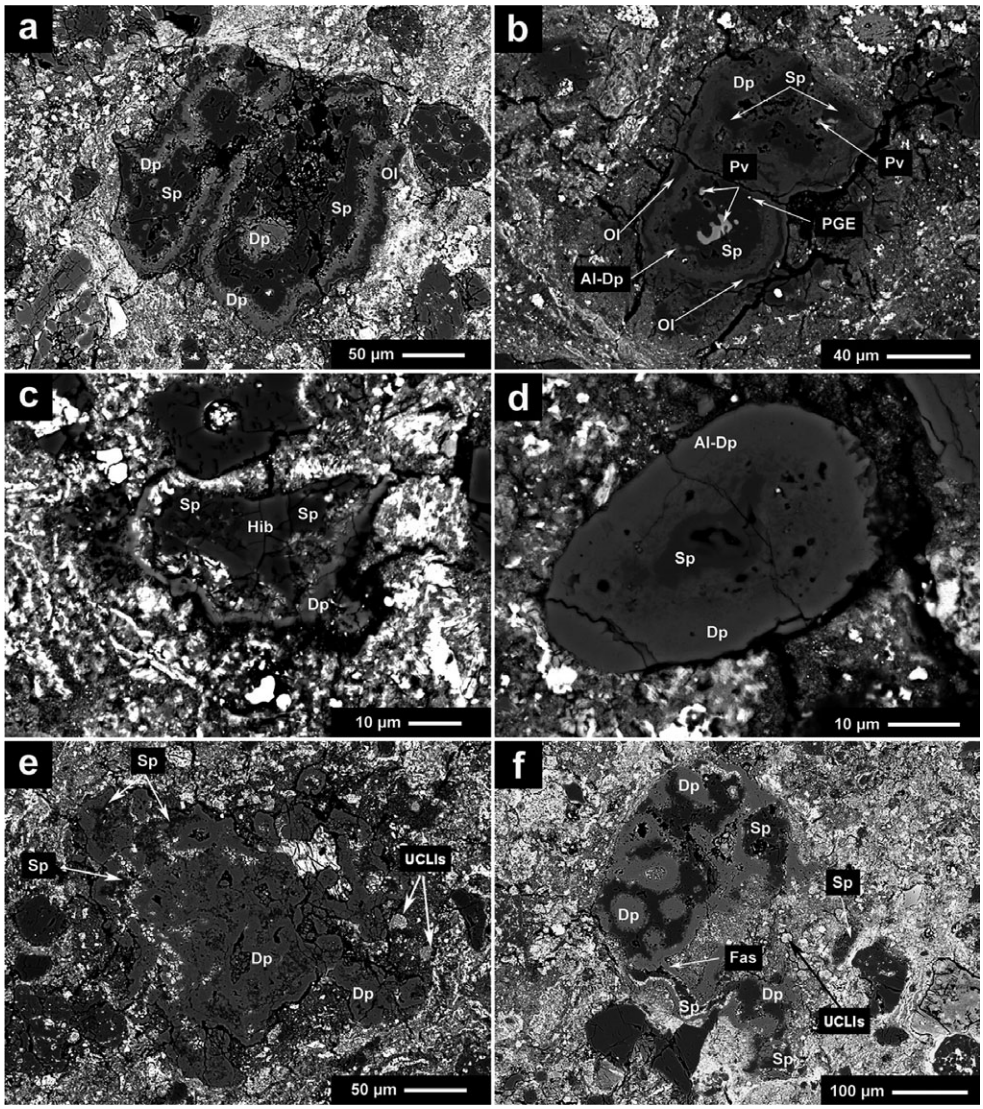

Fig. 7. Backscattered electron images of six Ca,Al-rich inclusions. a) CAI A-D3-2 is a fine-grained CAI with mainly spinel in the interior and a partly fragmented diopside and olivine rim; b) CAI B-A4-1 contains spinel, diopside, olivine, perovskite, Al-diopside, and a PGE-nugget (Ir,Os,Mo,Ru-nugget); c) A-C2-1 is a fragmented CAI with mainly spinel, diopside, and hibonite; d) CAI B-B6-3 is a relative small inclusion with spinel in the core and a diopside/Al-diopside rim; e) Inclusion A-C3-1 shows a contorted/sinuous appearance with mainly diopside and minor spinel; f) CAI B-B7-1 is a relative large inclusion containing spinel, diopside, and fassaite. ol = olivine; sp = spinel; dp = diopside; Al-dp = Al-rich diopside; fas = fassaite; hib = hibonite; pv = perovskite; PGE = platinum group elements.

the whole sample, but only occur as individual components within the FGRs and not in the matrix. Most of the UCLIs are small, round inclusions of <5–30 µm in diameter, but some are as large as 50 µm in size and irregularly shaped (Fig. 9a). Many UCLIs are surrounded by cracks and this feature clearly distinguishes them from the other constituents of the FGR. The UCLIs contain distinct mineral phases like "large" olivine and metal grains, which are clearly visible by SEM (Fig. 8b). The mineralogy of the UCLIs will be described in more detail in the TEM Investigations section.

The bulk composition of the UCLIs is similar to that of the FGR, but differs in the concentrations of S and Fe (Table 2). Also, the totals of the UCLIs (~95.3 wt%) are clearly higher than those for the FGR (~86.5 wt%).

Oxygen Isotopic System

Two pieces of the sample NWA 11024 were analyzed. The results compared with those of NWA 5958 (Jacquet et al. 2016) and Paris (Hewins et al. 2014) are shown in Fig. 10. The two bulk samples have a $\delta^{17}O$ of −1.60‰ and −1.44‰ and a $\delta^{18}O$ of 6.85‰ and

Table 3. Composition of various selected mineral phases in different CAIs from NWA 11024. See supporting information for more data (Table S5).

CAI	A-C3-1	A-D3-1	A-B3-2	B-A4-1	A-C1-3	B-A4-1	A-C2-1
Mineral	Diopside	Al-diopside	Fassaite	Spinel	Olivine	Perovskite	Hibonite
Na_2O	0.03	0.05	0.03	nd	0.03	nd	0.04
MgO	18.3	16.6	13.00	28.4	56.8	0.13	2.96
Al_2O_3	2.75	5.5	12.9	70.5	0.02	0.75	86.1
SiO_2	54.6	52.2	46.2	0.03	42.9	0.09	0.10
CaO	24.6	25.2	25.1	0.12	0.10	39.8	7.9
TiO_2	0.03	0.42	2.32	0.93	0.03	57.1	2.17
FeO	0.74	0.30	0.80	0.25	0.87	0.34	1.05
MnO	0.04	<0.01	nd	0.03	0.19	0.04	nd
NiO	nd	0.05	0.03	<0.02	nd	nd	0.08
CoO	nd	nd	nd	nd	<0.01	nd	<0.02
ZnO	0.18	0.22	0.17	nd	0.19	<0.02	0.16
Cr_2O_3	0.05	0.06	0.12	0.21	0.17	nd	0.04
Total	101.0	100.4	100.4	100.5	100.9	98.3	100.4
En	50.2	47.6					
Wo	48.6	51.9					
Fo					99.1		

nd = not detected.

6.07‰, respectively. Both measured samples plot in the ^{16}O-rich area of the CM field.

Bulk Chemical Analyses

The bulk main and trace element compositions compared with NWA 5958 and Paris are listed in Table 4. Since the Si concentration was not determined, SEM-EDS was additionally used to determine the bulk composition (and Si in particular) of thin section A. The measured SEM-EDS results for the major elements are similar to the values obtained by ICP-AES and ICP-SFMS. One exception is the FeO value measured by EDS which is somewhat lower. This may be due to the lack of large weathered (or unweathered) metal grains within the randomly set and analyzed areas.

The bulk sample contains 31.0 wt% SiO_2, 33.1 wt% FeO, 24.3 wt% MgO, and 2.5 wt% Al_2O_3 which are higher than those for Paris and NWA 5958 but are still in the range of CM chondrites. Normalized to CI, the three samples show a very similar pattern (Fig. 11) except for K, Na, Ba, Sr, and U. NWA 5958 and NWA 11024 have slightly higher K values than Paris, while NWA 11024 shows low Na contents. The different K and Na concentrations could result from different degrees (duration) of terrestrial weathering. Alternatively, this characteristic is due to different locations during the weathering episodes. For example, Haack et al. (2012) concluded that CM chondrites are depleted in Na, if exposed to rain. Considering the trace element abundances, NWA 11024 shows a relatively flat pattern, except for Sr, Ba, and U. Sr is ~7 times, Ba is ~38 times, and U is 6.5 times enriched compared to CI chondrites. This is typical for terrestrially weathered samples (Stelzner et al. 1999). The distinct depletion of the moderately volatile elements (e.g., Na, Zn, Ga, Rb, and Cs) may also reflect the high degree of terrestrial weathering.

Hysteresis Properties and Magnetic Susceptibility

Hysteresis properties of NWA 11024 are similar to those of other CM2 falls with a magnetic grain size in the pseudo-single domain range (Fig. 12). However, because these parameters are sensitive to both grain size and magnetic mineralogy (metal and magnetite relative abundance), the comparison remains qualitative. Saturation magnetization is five times higher than that of CM falls, and similar to that of Paris. It indicates a metal content of 2.1 wt% (this is the maximum value computed considering that there is only metal and no magnetite within the sample). The magnetic susceptibility is also higher than that for CM falls and similar to the value of Paris.

The ratio of saturation magnetization to ferromagnetic susceptibility, which can be used as a qualitative proxy to evaluate the dominance of metal versus magnetite, is $2.21(\pm0.20) \times 10^5$ for the two thin sections, and 1.98×10^5 for the measured bulk sample of NWA 11024. For Paris, this ratio is $2.28 (\pm0.46) \times 10^5$ (average of nine samples), and $1.09 (\pm0.28) \times 10^5$ for seven CM2 falls (data from Cournede et al. 2015). Theoretical values for multidomain metal and magnetite are 4.12×10^5 and 1.53×10^5, respectively (note that these theoretical values are grain size dependent). For comparison, H and L chondrites

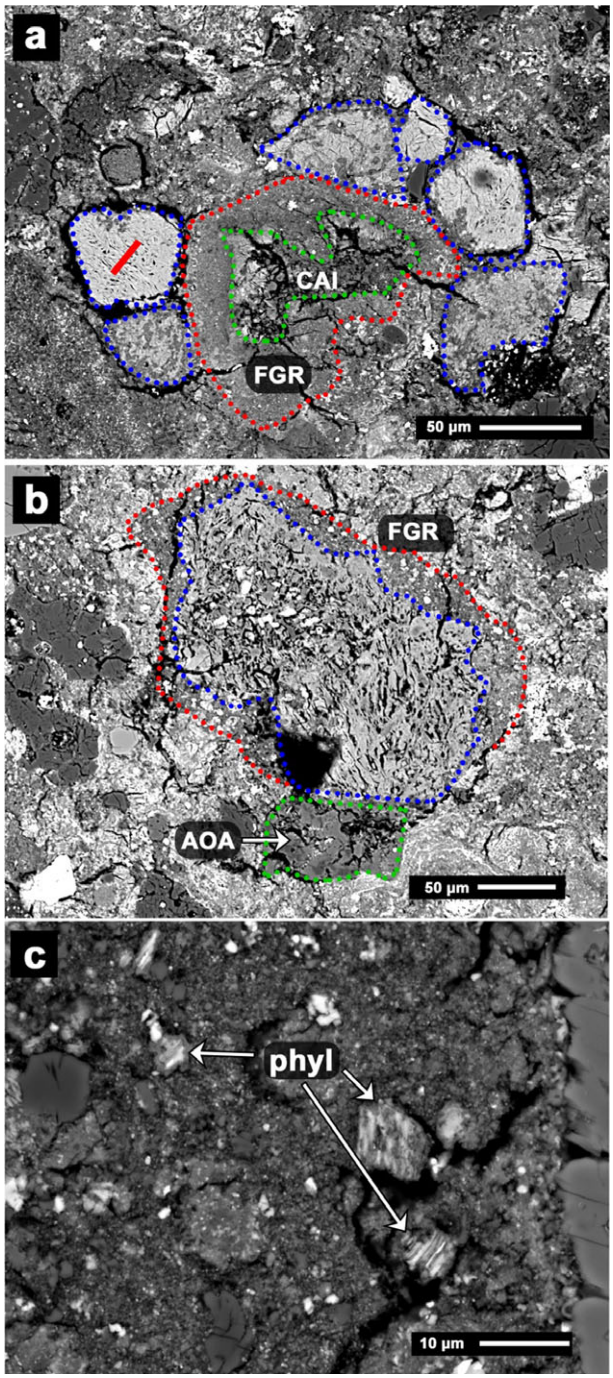

Fig. 8. Backscattered electron images: a) TCI-1 pseudomorph: Aggregate of different former TCIs (blue dotted lines) surrounding a fragmented CAI (green dotted line). The red solid line marks the area of the FIB section. The red dotted line indicates the FGR around the CAI. b) TCI-2 pseudomorph: A single TCI pseudomorph (blue dotted line) partly surrounded by a FGR (red dotted line) and an AOA (green dotted line). c) Three small phyllosilicate pseudomorphs (<10 µm) in a fine-grained rim. phyl: phyllosilicate pseudomorphs; AOA = amoeboid olivine aggregate; FGR = fine-grained rim; CAI = Ca,Al-rich inclusion. (Color figure can be viewed at wile yonlinelibrary.com.)

that have Fe,Ni metal and no magnetite give a ratio of 2.32×10^5 (measured on 56 falls; Gattacceca et al. 2014). This shows that the magnetic mineralogy of NWA 11024 is similar to that of Paris, and is more metal rich than that of other CM chondrites.

Raman Spectroscopy

The carbon embedded in the matrix can be used to estimate the peak temperatures a meteorite has seen in its evolution. The ability of Raman spectroscopy was applied to the structural change of carbonaceous material with higher temperatures to produce a geological thermometer. One hundred and twenty-seven measurements were performed in which the FWHM of the D1-band (Fig 13a) varied from ~160 to ~140 cm^{-1} with an average of 150 cm^{-1} (Fig. 13b). Using the correlation (Equation 1) obtained by Homma et al. (2015), an average peak temperature of the carbonaceous material is estimated to be 16 ± 30 °C (1σ).

X-Ray Diffraction

The X-ray diffraction between 5 and 22 2ϑ (°) shows no peaks at ~8.1 and ~16.2 2ϑ (°) (Fig. 14), where the strongest reflections of phyllosilicates would be. A small reflection appears at ~17.2° (forsterite) and a distinct one at ~21.4° (main peak of goethite). Heated CM chondrites from stage II onwards in Nakamura (2005) show also no peak, whereas unheated/stage I samples have a prominent peak for serpentines.

TEM Investigations

Two FIB samples were obtained from a fine-grained rim (FGR) including an UCLI (Figs. 9, 15, and 16), and a complex aggregate showing a typical phyllosilicate-related morphology (TCI-1, Fig. 8a).

The normal portion of the FGR sample shows a heterogeneous, porous mixture of olivine, pyroxene, Ni-rich metal, and Fe-sulfide grains (the largest identified as troilite). In between the well-formed grains, a nanocrystalline phase occurs that yields ring patterns in selected area electron diffraction (SAED) matching the lattice spacings of olivine. Neither the characteristic lattice spacings of phyllosilicates nor substantial amounts of amorphous material could be detected. However, the presence of small amounts of amorphous material cannot be completely ruled out.

TEM-EDS analysis of the UCLIs (Table 5) indicates that the nanocrystalline material is Fe-rich and that its molar Si/(Mg+Fe) is typically >0.5 as expected for olivine. This may be indicative of the presence of some Si-rich, amorphous material. The enrichment of

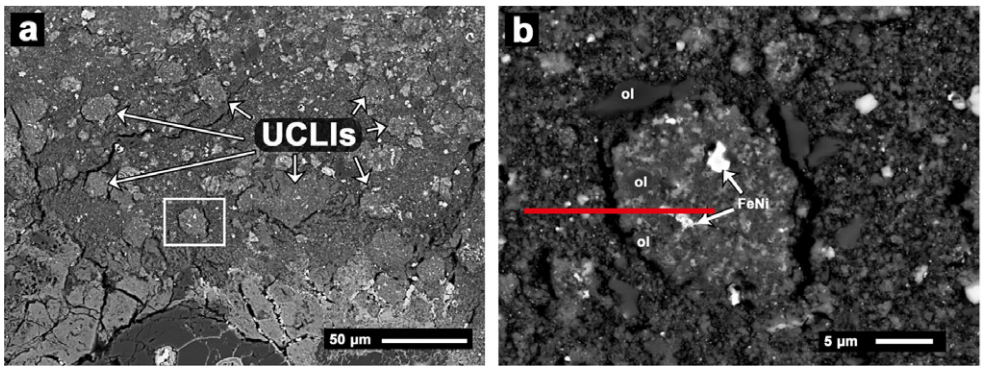

Fig. 9. Backscattered electron images: a) Part of a FGR surrounding a type Im chondrule. The UCLIs (arrows) are clearly visible in the rim. The white square marks the UCLI from Fig. 8b. b) Typical UCLI with a fine-grained matrix containing olivine and metal grains. The red line marks the position of the FIB section. ol = olivine; FeNi = Fe,Ni metal. (Color figure can be viewed at wileyonlinelibrary.com.)

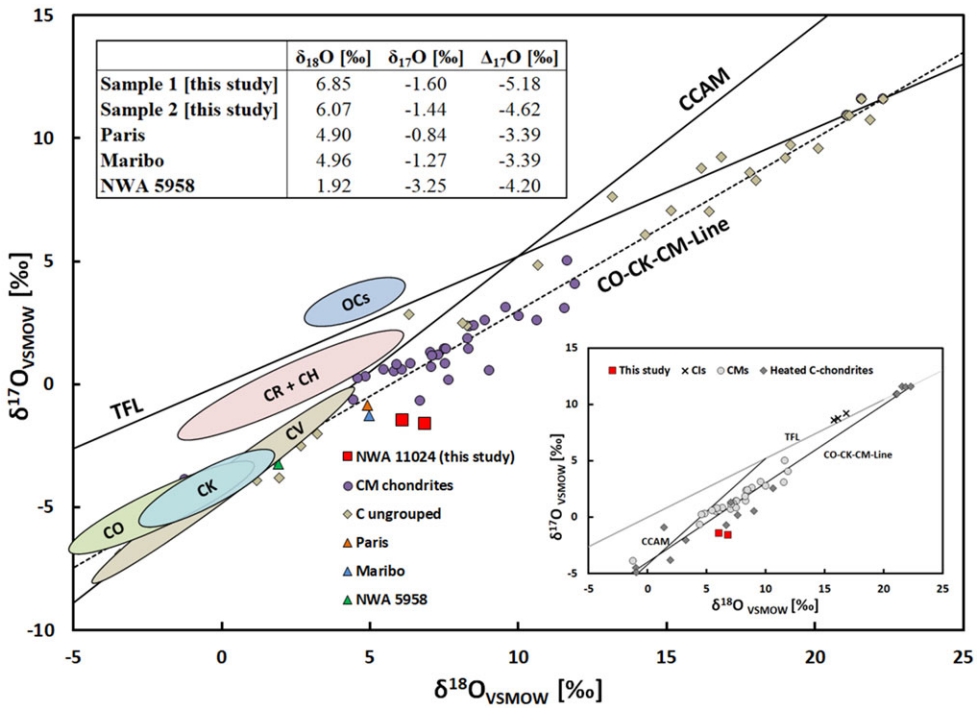

Fig. 10. Oxygen isotope composition of two aliquots of NWA 11024 (black squares). The table shows the results compared to Paris (Hewins et al. 2014), NWA 5958 (Jacquet et al. 2016), and Maribo (Haack et al. 2012). Data for O-isotopes of other C-chondrites are from Clayton and Mayeda (1999), Greenwood et al. (2010 and references therein), and Tonui et al. (2003). (Color figure can be viewed at wileyonlinelibrary.com.)

Fe in the fine-grained material contrasts with the very Mg-rich olivine and pyroxene present as large, well-formed grains (Mg#: 98–99 mol%). The nanocrystalline olivine in the fine-grained material is accompanied by grains of Ni-poor Fe-sulfide and Ni-rich metal (~$Fe_{50}Co_3Ni_{47}$) reaching sizes in the range of several 10s to 100s of nm.

The nanoscale mineralogy of the clot-like structures within the sampled FGR is very similar to the normal portion of the FGR and differences mainly exist in the quantitative modal abundance of phases. TEM-EDS shows a slightly larger Fe/(Mg+Fe) ratio and less Si-enrichment relative to the normal fine-grained material surrounding the UCLIs (Table 5). Fe-sulfide (most probably troilite) is more abundant and metal grains are nearly absent within the clot-like object, with the exception of one large, highly irregularly shaped Ni-rich metal grain (~1500 nm; Fig. 16, top row). The

Table 4. Major and trace element bulk composition of NWA 11024 (this study) compared to those of Paris (Hewins et al. 2014), NWA 5958 (Jacquet et al. 2016), and CM mean (Lodders and Fegley 1998).

wt%	This study Brest	This study EDS	Paris	NWA 5958	CM mean	ppm	This study	Paris	NWA 5958	CM mean
SiO_2	nd	31.0	28.7	29.4	30.5	Nb	0.44	0.38	0.39	0.40
TiO_2	0.13	0.10	0.10	0.11	0.09	Cs	0.07	0.13	0.12	0.11
Al_2O_3	2.56	2.32	2.07	2.25	2.14	Ba	93.7	3.24	21.9	3.10
FeO	33.1	29.0	25.6	24.7	27.17	La	0.37	0.33	0.56	0.32
MnO	0.27	0.25	0.22	0.22	0.21	Ce	0.95	0.83	1.27	0.94
MgO	24.3	23.6	19.8	20.1	19.07	Pr	0.14	0.13	0.19	0.14
CaO	1.67	1.65	1.61	1.31	1.80	Nd	0.72	0.64	0.88	0.63
Na_2O	0.19	0.38	0.67	0.54	0.53	Sm	0.23	0.21	0.26	0.20
K_2O	0.10	0.12	0.04	0.09	0.04	Eu	0.09	0.08	0.09	0.08
P_2O_5	0.32	0.42	0.28	0.34	0.24	Gd	0.33	0.29	0.32	0.29
ppm						Tb	0.06	0.05	0.06	0.05
Li	2.9		1.6	2.8	1.5	Dy	0.41	0.35	0.38	0.33
Be	0.03		0.03	0.04	0.04	Ho	0.09	0.08	0.08	0.08
Sc	10.4		8.38	8.04	8.20	Er	0.26	0.23	0.24	0.22
V	80.7		72.1	68.5	75.0	Tm	0.04	0.04	nd	0.04
Co	660		651	586	560	Yb	0.25	0.23	0.24	0.22
Cu	144		128	110	130	Lu	0.04	0.03	0.03	0.03
Zn	159		180	143	180	Hf	0.16	0.14	0.15	0.18
Ga	8.4		7.7	7.8	7.6	Ta	0.02	0.02	0.02	0.02
Rb	1.3		1.7	1.0	1.6	W	0.12	0.09	0.14	0.16
Sr	52.1		10.8	39.8	10.0	Pb	1.89	1.51	1.67	1.60
Y	2.6		2.1	2.3	2.0	Th	0.04	0.04	0.06	0.04
Zr	5.8		4.8	4.5	7.0	U	0.05	0.01	0.05	0.01

nd = not determined.

nanocrystalline olivine is more densely packed with correspondingly less pore space in the UCLIs compared with olivine in the surrounding fine-grained rim.

The FIB sample obtained from the apparent phyllosilicate aggregate shown in Fig. 8a yielded SAED ring patterns (Fig. 17) fully consistent with nanocrystalline olivine. EDS analysis shows that this material is highly enriched in iron (~Fa_{90}). Although even at the TEM scale the aggregate strongly resembles a phyllosilicate, no characteristic lattice spacing of cronstedtite or similar phases were detected. The grain size of individual olivine crystals is on the order of 10–100 nm. Besides the dominant Fe-rich olivine, only minor amounts of Fe-sulfide (most probably troilite) were found.

DISCUSSION

Classification of NWA 11024

After preparing two polished thin sections, the sample was recognized to be a carbonaceous chondrite based on the high abundance of fine-grained material (dust rims, matrix). Additionally, the oxygen isotope data show that it is related to the CM chondrite-forming region. However, phyllosilicates and calcite grains are missing and NWA 11024 was accepted by the Nomenclature Committee as an anomalous CM chondrite. Whether NWA 11024 is indeed a CM chondrite or an unusual carbonaceous chondrite needs to be clarified.

Chondrules, CAIs, and other components are embedded in an optically dark matrix, which makes up ~64 vol% (matrix and FGR). The abundance is quite similar to abundances of fine-grained components in other CM chondrites (e.g., McSween 1979a; Metzler et al. 1992). Therefore, it is clear that NWA 11024 is a carbonaceous chondrite and the abundance of fine-grained material speaks for a CM chondrite. The oxygen isotopes plot in the ^{16}O-rich area of the CM field. Many (not all) of the heated CM chondrites tend to plot on the right side of the CO-CK-CM line (Fig. 10) similar to NWA 11024. Most of the CAIs are small (<100 μm) and characterized by a core of spinel and a Ca-pyroxene rim. The size distribution, mineralogy, and the abundance (~1.2 vol%) are in good agreement with those of other CM chondrites (Brearley and Jones 1998; Rubin 2011; MacPherson 2014). Large CAIs are missing and none of the 82 studied CAIs contains melilite, which is different from CAIs in CO chondrites that typically contain

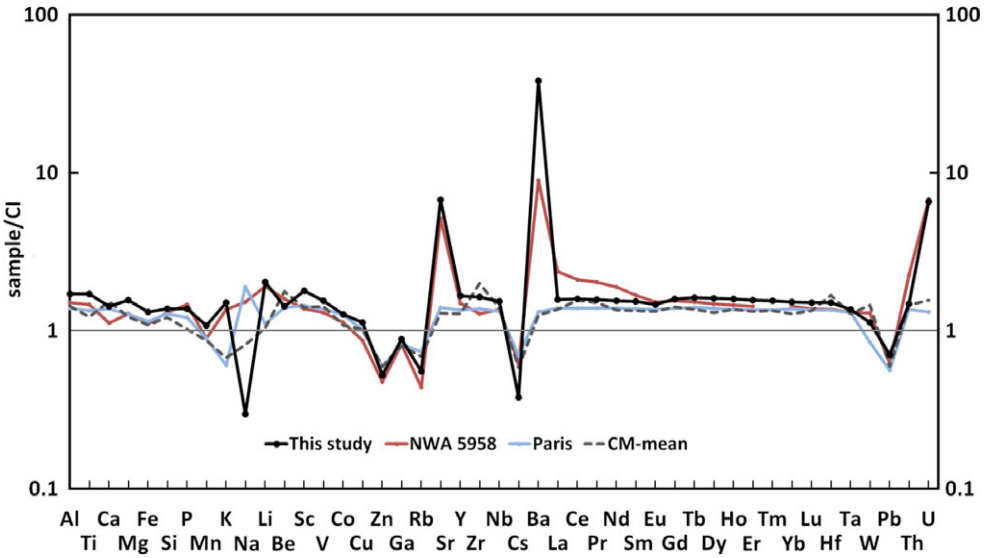

Fig. 11. CI-normalized bulk composition of NWA 11024 compared to those of NWA 5958 (Jacquet et al. 2016), Paris (Hewins et al. 2014), and CM mean values (Lodders and Fegley 1998). CI values are from Barrat et al. (2012). (Color figure can be viewed at wileyonlinelibrary.com.)

melilite (Brearley and Jones 1998). CAIs from CV chondrites are typically larger than in NWA 11024 (MacPherson 2014) and the modal abundance is too low compared with CV chondrites (~3.0 vol%; Rubin 2011).

The bulk Al/Mn and Zn/Mn ratios of different meteorite groups plot in distinct compositional clusters (e.g., Kallemeyn et al. 1996). NWA 11024 plots together with NWA 5958 and Maribo next to the CM field (Fig. 18) and clearly aside from other carbonaceous chondrite groups. Furthermore, the magnetic (hysteresis) properties of NWA 11024 are similar to those of other known CM2 falls or the CM chondrite find Paris. All these different results points clearly to a CM chondrite classification of this rock.

Since the olivines do not show undulatory extinction and most of the Ni-poor metals are destroyed, the degrees of shock metamorphism and weathering are S1 (according to the scale of Scott et al. 1992) and severe (W3, using the classification scheme for ordinary chondrites of Wlotzka 1993), respectively.

Unknown Clot-Like Inclusions

NWA 11024 shows significant differences to other known CM chondrites. One remarkable feature is the occurrence of unknown clot-like inclusions (UCLIs). They are found most prominently in the fine-grained rims of the type Im chondrules, but are also present in the fine-grained rims of other chondrules and CAIs.

The bulk composition of UCLIs differs from the surrounding FGR mainly by their higher S and Fe values (Tables 1, S3, and S4) caused by a quantitative higher modal abundance of troilite (Figs. 15 and 16). Furthermore, the UCLIs have a higher density resulting in analytical totals of ~95 wt%, whereas FGRs show totals of ~86.5 wt% (Table 2).

Similar inclusions in the FGR of the meteorite Elephant Moraine 96029 were described by Lee et al. (2016) as compact and amorphous/nanocrystalline patches of some μm in size. Analogous patches are present in the matrix of the weakly altered fragments within the Paris breccia (Hewins et al. 2014). Lee et al. (2016) concluded that these patches were probably nebular in origin. The preservation of this primitive material shows that some components escaped aqueous alteration speaking for a weakly altered sample.

Furthermore, Chizmadia and Brearley (2008) described heterogeneities in the FGR of Y-791198 at the submicron scale that are divided into distinct S-rich and S-poor regions which appear as irregularly shaped regions of 0.2–0.5 μm in size. The two regions differ mainly in little variation of their mineralogy, texture, and grain sizes. This description is very similar to the characteristics of UCLIs compared to the FGRs. This leads to the assumption that the small areas described by Chizmadia and Brearley (2008) are related to the UCLIs in NWA 11024; even the UCLIs are larger and more distinct than those in the FGR of Y-791198. The S-rich regions in Y-791198 contain also serpentine, which is not present in the UCLIs in NWA 11024. As will be discussed below in more detail, this can be caused by a heating event on the parent body of NWA 11024, which decomposed the phyllosilicates to Fa-rich olivine and troilite. This is also an argument in order to explain why

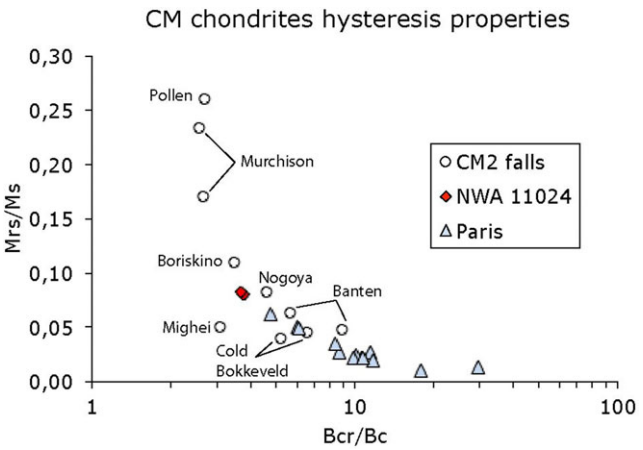

Fig. 12. Magnetic hysteresis parameters for NWA 11024 and comparison with other CM chondrites. Data for Paris are from Hewins et al. (2014). Data for CM falls are from Cournede et al. (2015). (Color figure can be viewed at wileyonlinelibrary.com.)

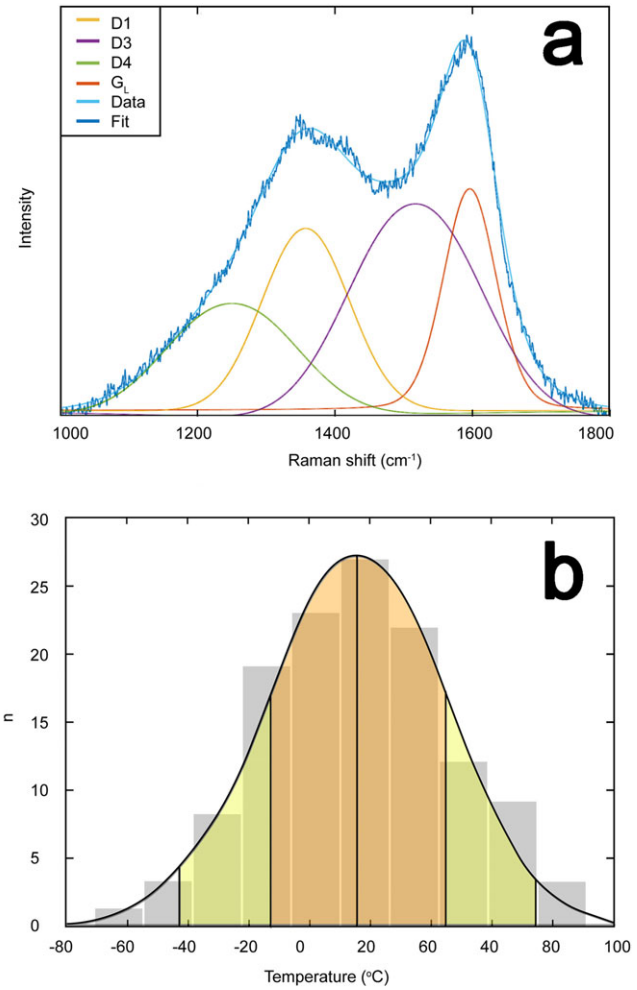

Fig. 13. a) An example spectrum of carbonaceous material in the NWA11024 matrix. The fit is a result of the accumulation of four pseudovoigt bands. b) The 127 obtained Raman temperatures show a Gaussian distribution with an average of 16 ± 30 °C (1σ). (Color figure can beviewed at wiley onlinelibrary.com.)

the nanocrystalline material in the UCLIs is more Fe-rich than "larger" olivine and pyroxene grains (see the Results of the TEM Study section) and also why troilite is more abundant within the UCLIs than in the surrounding FGR.

It has to be mentioned that a heating event may have caused S-loss of some regions within the FGR. But in this case, a gradual depletion of sulfur from the inner to the outer part of the FGR must be present. However, this is not the case. The UCLIs are present as small patches in the outer and inner part of the FGR. Furthermore, it may be speculated that the UCLIs represent initial stages of aqueous alteration of the FGR material, which formed phyllosilicates and tochilinite–cronstedtite intergrowths (TCI), which subsequently decomposed to produce nanocrystalline Fa-rich olivine and troilite. This pathway may explain the visually larger bulk density, smaller grain size, and the higher abundance of sulfide grains in the unknown clot-like structures (Fig. 9). The olivine, pyroxenes, and the metal grains in the FGR had also to be generated by the heating event, which would require at least 750 °C (see next paragraph for more details). Such a process would not explain the compositional differences (especially in sulfur) between the UCLIs and the rest of the FGRs. Therefore, the unknown clot-like inclusions must be of primary origin and have been present in the FGRs before the accretion on the parent body.

Chizmadia and Brearley (2008) also concluded that the S-rich and S-poor patches were formed as individual objects in the solar nebula. They accreted together with other fine-grained components to form the fine-grained rims. As a consequence, the FGRs are accretionary dust mantles as described in Metzler et al. (1992). However, S-rich and S-poor dust cannot be formed in the same location of the solar nebula (Chizmadia and Brearley 2008) and consequently, the UCLIs and the rest of the fine-grained material were mixed together from two different regions.

Possible source objects for the UCLIs could be interplanetary dust particles (IDPs), which was also assumed for the amorphous material in the FGR of Y-791198 (Chizmadia 2005; Chizmadia and Brearley 2008). There are different types of IDPs and the best fitting are chondritic and cometary IDPs which are similar in size and composition. They are between 5 and 30 μm large porous aggregates containing mainly pyroxene (enstatite), olivine (forsterite), Fe-rich sulfides, amorphous material, and different phyllosilicates (Bradley 1988, 1994). They are seen as dust or debris

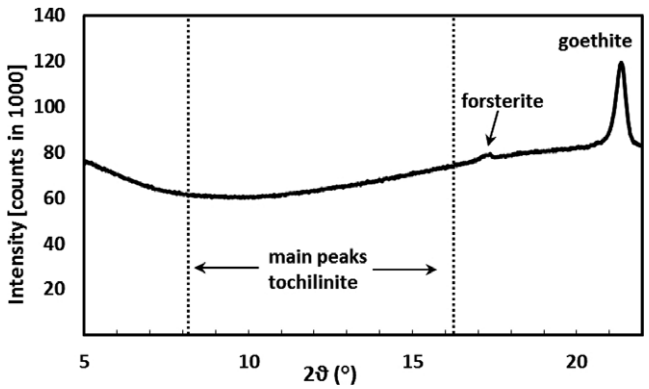

Fig. 14. X-ray diffraction pattern obtained from a piece of NWA 11024. No reflection related to the occurrence of tochilinite is visible (dotted lines). A small reflection of forsterite (~17.3°) is present as well as the main peak of goethite (~21.4°).

from comets, icy asteroids, Main Belt asteroids, or protoplanets (e.g., Bradley 1994; Rietmeijer 1998). One difference is the occurrence of the Ni-rich metals in the UCLIs, while Ni-poor taenite is common in most described IDPs (e.g., Fraundorf 1981; Rietmeijer 1998). But still, small particles of ice-rich asteroids or icy bodies are a plausible source for the UCLIs.

Finally, a heating event decomposed the small phyllosilicates in the unknown clot-like inclusions after the accretion in the FGR (most possible on the final parent body). Such a heating process could produce a high total density, decompose the phyllosilicates to Fa-rich olivine and troilite, and trigger the formation of shrinking cracks around many UCLIs. Thus, it is important to know the heating source and which peak temperatures could have been responsible in order to explain the mineralogical and chemical characteristics within the sample.

Source of Heating Process

Different heating sources are possible. They include shock-induced heating caused by impacts, solar irradiation, or heating by radioactive decay of short- and long-lived radioisotopes. Impacts and collisions between larger bodies were one of the fundamental processes in the early solar system (Shoemaker 1977). However, Scott et al. (1992) reported that the least shocked chondrite groups are CM2 and CO3: 36 out of 38 members are classified as shock stage S1 (<5 GPa), and only one CM2 chondrite was shocked to stage S2. The shock stage of S2 would indicate an equilibrium shock pressure of 5–10 GPa (Stöffler et al. 1991, 2018; Bischoff and Stöffler 1992).

Stöffler et al. (1991) and Scott et al. (1992) have suggested that the deficiency of strongly shocked petrologic type 2 (carbonaceous) and type 3 (carbonaceous and ordinary) chondrites is due to a higher porosity than found in type 4–6 chondrites. In addition, in case of the carbonaceous type 2 chondrites, the high abundance in volatiles may be responsible for different responses to shock compression. Experiments of Tyburczy et al. (1986) have demonstrated that Murchison can be partially devolatilized by shock pressures of 11 GPa and experience total devolatilization at 30 GPa. Although the higher degree of porosity of type 2 chondrites may cause higher post-shock temperatures (and therefore melting at lower pressures) and the higher volatile contents can disperse more easily in the shocked rocks (Scott et al. 1992), distinct shock features in olivine (undulatory distinction and planar fractures at pressures between 5 and 15 GPa) must be recognized already during shock processes leading to partial devolatilization. Moreover, moderate, yet nondisruptive, shock compression is expected to result in considerable compaction by the collapse of intergranular pores. In contrast, NWA 11024 exhibits no shock features in olivine, preserves a remarkably high degree of porosity in the FGRs, and does not show evidence for uniaxial compression (e.g., by flattened chondrules). Based on these observations, we exclude significant heating and losses of volatiles due to shock loading.

As impacts can be excluded, radioactive decay and solar heating remain as likely sources of heating. Long- and short-lived isotopes were an important heat source in early formed planetesimals and were able to create the temperatures necessary for aqueous alteration and thermal metamorphism (Gail et al. 2014). It is possible that material from deeper regions of a CM parent body experienced higher temperatures than material closer to the surface, similar to the onion shell model of ordinary chondrites. Also possible is heating by solar irradiation during low perihelion passages of either the parent body of NWA 11024 or its meteoroid. This would have induced one or more relatively short-temperature excursions that would have primarily affected the topmost surface of the body. The depth of thermal effects depends on the orbital parameters, size, and surface material of the body (e.g., Michel and Delbo 2010).

Thus far, no decisive criteria have been established to differentiate heating processes, but peak temperature and duration are obviously important parameters that can be estimated from petrological observations.

Thermal Annealing of C Chondrite Parent Bodies and Determination of the Peak Temperatures

The peak temperatures a rock has experienced during thermal annealing can be determined by different

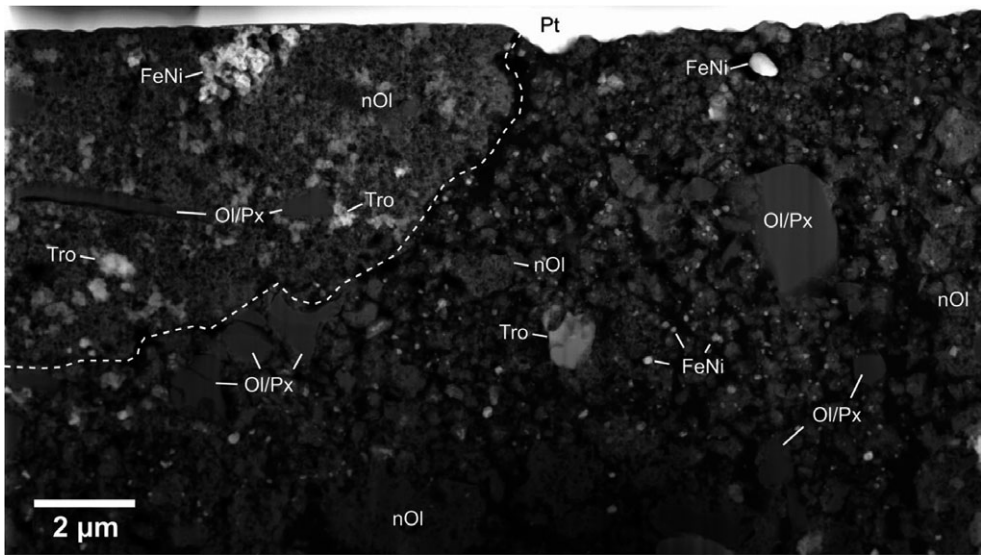

Fig. 15. STEM-HAADF image of the FIB section obtained from the FGR shown in Fig. 9. The dashed line marks the extent of the clot-like structure (upper left) observed in BSE images. Internally, this region is denser packed compared to the normal FGR material. Ol/Px = olivine or pyroxene, nOl = nanocrystalline olivine, Tro = troilite, FeNi = Ni-rich taenite, Pt = platinum protective cover.

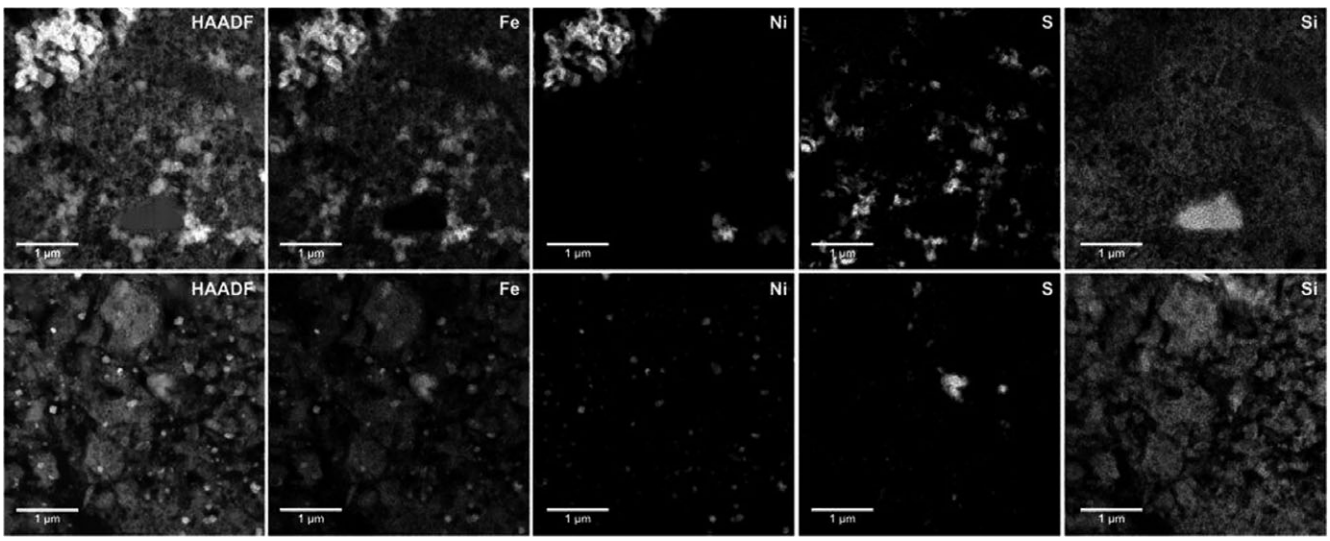

Fig. 16. STEM-HAADF and -EDS X-ray maps of the UCLI in Figs. 9 and 15 (top row) and the normal FGR material (bottom row).

techniques. One way is to investigate mineral phases produced by a heating event as different temperature ranges decompose phases and create new minerals or parageneses.

Considering the metallic particles within the normal FGR and the UCLIs, these may have been produced by the thermal decomposition of Fe,Ni sulfides, similar to the observed analogues in the thermally metamorphosed CM-like chondrites Yamato (Y-)86720 and Belgica (B-)7904 (Harries and Langenhorst 2013), as well as in many other heated CM-like chondrites (e.g., Bischoff and Metzler 1991; Nakamura 2005). Y-86720 and B-7904 belong to the heating stage IV of Nakamura (2005), which corresponds to a temperature of >750 °C during a brief heating event. However, in Y-86720 and B-7904, the newly formed metallic particles are Ni-poor (~6 atom%), while those observed here are generally Ni-rich (~$Fe_{50}Ni_{50}$).

Table 5. Representative TEM-EDS analyses of finegrained material in the FIB-sampled FGR and UCLI (normalized to a total of 100%).

FGR at%	1	2	3	4	5	6	7
O	57	58	59	59	59	60	61
Mg	18	15	14	13	18	16	12
Al	1.4	1.8	1.6	2.0	1.9	2.2	2.5
Si	14	15	17	24	16	19	21
Fe	9.1	10	9.1	2.3	5.1	3.2	3.1
Mg# mol%	**67**	**60**	**60**	**85**	**78**	**83**	**80**
Si/(Mg + Fe)	**0.5**	**0.6**	**0.7**	**1.6**	**0.7**	**1.0**	**1.3**
UCLI at%	**8**	**9**	**10**	**11**	**12**	**13**	**14**
O	58	59	58	59	58	59	60
Mg	11	13	13	10	14	13	12
Al	1.7	1.5	1.9	1.6	1.8	1.9	2.2
Si	15	18	16	16	15	17	18
Fe	13	8.4	10	13	11	9.3	8.1
Mg# mol%	**45**	**61**	**57**	**43**	**57**	**59**	**60**
Si/(Mg + Fe)	**0.6**	**0.8**	**0.7**	**0.7**	**0.6**	**0.7**	**0.9**

This suggests that the loss of S may have happened at lower temperatures, because Ni-rich sulfides such as pentlandite are expected to be thermally less stable than FeS based on their thermodynamic properties (Waldner and Pelton 2004). The actual temperature of decomposition strongly depends on the sulfur fugacity of the system, which can be constrained by the coexistence of troilite (tro) and Fe,Ni metal based on the equilibrium:

$$FeS_{(tro)} = Fe_{(in\ Fe50Ni50)} + 0.5S_{2(g)}$$

This allows estimating the minimum temperature of pentlandite decomposition based on the assumption that any initially present pentlandite (pn) had a similar Fe/Ni ≈ 1 ratio as observed in the metal. The applicable equilibrium is:

$$Fe_9S_{8(in\ pn)} = 9Fe_{(in\ Fe50Ni50)} + 4S_{2(g)}$$

With the appropriate thermodynamical data and activity coefficients for Fe in metal and in pentlandite (Hillert and Qiu 1991; Waldner and Pelton 2004, 2005), the resulting minimum temperature is ~280 °C. Above this temperature, pentlandite with the composition of $Fe_{4.5}Ni_{4.5}S_8$ may not coexist with $Fe_{50}Ni_{50}$ metal in the presence of troilite. Because pentlandite has not been observed in the FGR or UCLIs, more detailed constraints are not possible to consider. This reveals that a heating event with a minimum temperature of ~280 °C must have taken place.

Another way to determine the peak temperature is the classification scheme for heated carbonaceous chondrites from stage I–IV defined by Nakamura (2005). This system is mainly based on X-ray diffraction analyses of the phyllosilicates in the matrix. Combined with heating experiments on Murchison by Akai (1992), stage I shows no phase changes below 300 °C. About 300–500 °C (stage II) are necessary that serpentine (Akai 1990b, 1992; Zolensky et al. 1993) and tochilinite start to decompose (Gooding and Zolensky 1987) and a transitional structure of serpentine and olivine appears. Between 500 and 750 °C (stage III), olivine starts to crystallize increasingly growing with higher temperature. Above 750 °C (stage IV), low-Ca pyroxene begins to crystallize (Nakamura 2005). Considering the presence of pristine troilite (not decomposed to Ni-poor metal), the dehydration of initially present phyllosilicates, and crystallization of micro-olivine and no low-Ca pyroxene, the heating of NWA 11024 may be constrained to stage III (500–750 °C) rather than stage IV of Nakamura (2005).

As the olivines within the sample show various compositions from $Fo_{>99}$ to Fo_{37} (Fig. 5), the metamorphism at temperatures above 700 °C must have been extremely short, otherwise the range in olivine compositions could not survive. Furthermore, during prolonged heating at ~600 °C, the rims of chondrules and chondrule/olivine fragments start to interact with the matrix, resulting in blurring effects on their edges (Tonui et al. 2014). This is not visible in NWA 11024 and 600 °C can be seen as an upper limit of thermal annealing on long time scales compatible with radiogenic heat production at depth within the parent body. Because no phyllosilicates are preserved in chondrules, yet no blurring effects at chondrule rims are present, we suppose a heating event at temperatures between 400 and 600 °C if it occurred on long time scales. Note that shorter heating duration would allow for higher peak temperatures, because textural equilibration and the blurring of original structures is a slow process. The temperature predicted for a longer heating event is in good agreement with the temperature estimates of 400–600 °C for the mildly aqueously altered and heated CM carbonaceous chondrite EET 96029 (Lee et al. 2016) and 500 °C for the heated meteorite Y-793321 (Nakamura 2006).

This heating event in Y-793321 likely caused an increasing of the mean totals of the matrix to 92 wt% (Nakamura 2006). This was confirmed by heating experiments at 600 °C which increased the totals of Murchison's matrix from 80.7 wt% to 93.1 wt% (Nakato et al. 2008). These reported mean totals for matrices in other annealed CM chondrites are in a good agreement with the mean totals revealed during analyses of fine-grained constituents of NWA 11024. Therefore, for NWA 11024, we conclude a peak temperature of at least 400 °C, but not higher than 600 °C on long terms.

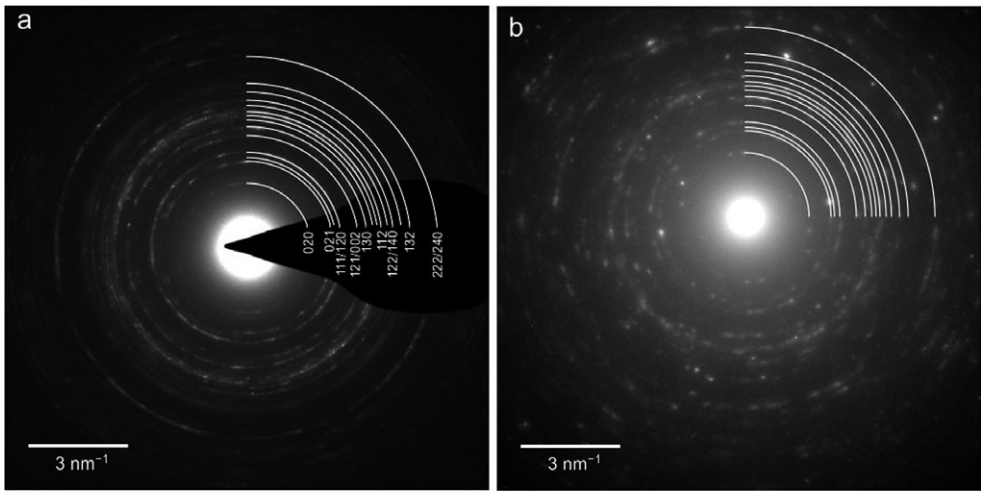

Fig. 17. TEM-SAED patterns. a) Pattern obtained from the phyllosilicate pseudomorph (TCI-1; compare Fig. 8a) showing partial rings indexed for olivine. No other phase than nanocrystalline olivine was detected. b) Pattern obtained from the clot-like structure in Fig. 15. Partial diffraction rings of nanocrystalline olivine dominate, other reflections belong to troilite.

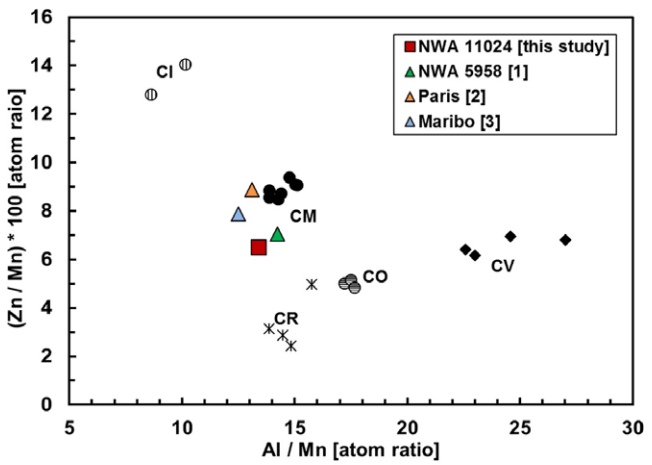

Fig. 18. Al/Mn versus Zn/Mn plot including the bulk composition of NWA 11024 compared with distinct clusters of different meteorite groups (Kallemeyn and Wasson 1981, 1982; Kallemeyn et al. 1994). NWA 11024 (red square) plots together with NWA 5958 and Maribo at the CM field. (Color figure can be viewed at wileyonlinelibrary.com.)

Because mildly heated CM2 chondrites such as Y-793321 do not contain abundant olivine formed from dehydrated phyllosilicates as observed in NWA 11024, a short-term temperature excursion above 600 °C, possibly by solar heating of the meteoroid, cannot be fully excluded.

Raman spectroscopy is another applicable technique to produce a geological thermometer (between 20 and 540 °C) due to the changes in the structures of carbonaceous material in chondrites with increasing temperature (Homma et al. 2015). The results of the Raman investigation show that carbonaceous material in NWA 11024 experienced a temperature of 16 ± 30 °C (1σ). These results contradict with the estimated peak temperatures obtained by matrix and chondrule textures that indicate a temperature of 400–600 °C. However, this temperature difference can be explained by the overall strong modification of the sample by terrestrial weathering. Severe weathering can cause the alteration or exchange of organic matter with terrestrial carbonaceous material (Sephton 2004; Bland et al. 2006; Busemann et al. 2007). Sephton (2004) mentioned that the organic matter inside meteorites is the most susceptible component to terrestrial weathering and that heavily weathered samples contain one order of magnitude less organic matter compared to less-altered samples. Busemann et al. (2007) detected changes of the Raman spectra in heavily weathered hot desert samples and proposed two theories as follows, suggesting either (1) an increased ordering in the structure of the inorganic matter observed by smaller D- and G-bands caused by terrestrial weathering or (2) the loss of fragile organic matter and the replacement by terrestrial organic matter. In rare cases, the complete absence of organic matter caused by terrestrial weathering can be observed (Busemann et al. 2007). The mismatch between the low temperatures obtained by Raman carbon thermometry and the higher temperatures obtained by the mineralogical considerations for the sample can thus most likely be explained by the loss of extraterrestrial carbonaceous matter and the replacement by terrestrial organic matter driven by terrestrial weathering.

Degree of Aqueous Alteration

The first phases produced by aqueous alteration are phyllosilicates and calcite grains. The meteorites Paris

and Maribo, having fragments of the least altered known CM materials, show large areas of TCI-clumps and contain calcite grains. However, both components are missing in the sample NWA 11024. This distinguishes NWA 11024 from all other known CM chondrites and also from different volatile-rich, dark inclusions in brecciated chondrites and achondrites which are linked to CM or CI chondrites (e.g., Endreß et al. 1994; Zolensky et al. 1996; Patzek and Bischoff 2015; Patzek et al. 2016, 2018; Fioretti et al. 2017).

Even these typical aqueous alteration phases are missing; NWA 11024 plots on the lower ^{16}O-rich part of the CM field. The phyllosilicates in CM chondrites were formed by the interaction of ^{16}O-rich anhydrous minerals with a ^{16}O-poor aqueous fluid and the single linear pattern strongly speaks for the interaction of two single reservoirs (Clayton and Mayeda 1999). Increasing the incorporation of a ^{16}O-poor fluid raise the grade of mixing and leads to a shift to the upper right ^{16}O-poor area of the CO-CK-CM line. Considering NWA 11024, this is not the case and NWA 11024 plots on the ^{16}O-rich part of the CM field together with the low-altered CM chondrites Maribo and Paris. This indicates a lower incorporation of ^{16}O-poor water for these meteorites, and thus, a lower degree of aqueous alteration.

Some components appearing like small phyllosilicates or TCIs (pseudomorphs; Fig. 8c) are present in NWA 11024, but all of them are dehydrated. The investigation by X-ray diffraction shows that phyllosilicates are not present anymore or only in a nondetectible portion. TEM investigations revealed that phyllosilicates recrystallized to Fe-rich micro-olivine, which was probably caused by thermal alteration in a temperature range of 400–600 °C. Calcite grains can also be destroyed by thermal alteration, but they survive heating at 600 °C and will not decompose below 890 °C (Deer et al. 1992; Nakato et al. 2008). This needed temperature is much higher than the estimated temperature for the parent rock of NWA 11024. Therefore, we conclude that no calcite grains were formed during aqueous alteration and that calcite grains were never present in NWA 11024. This speaks also for a very minor alteration effect caused by water in this rock.

A low degree of aqueous alteration is also supported by the high abundance of metal (also considering the terrestrial weathering products) with ~2.5 vol%. Metal is highly reactive to aqueous alteration creating complex intergrowth of Fe-hydroxides in an early stage of this process (Tomeoka and Buseck 1985). Consequently, a higher degree of aqueous alteration causes a lower metal content. The less-altered CM meteorites Paris and EET 99019 contain 1.2 vol% and 1.7 vol% of metal, respectively (Hewins et al. 2014; Lee et al. 2016).

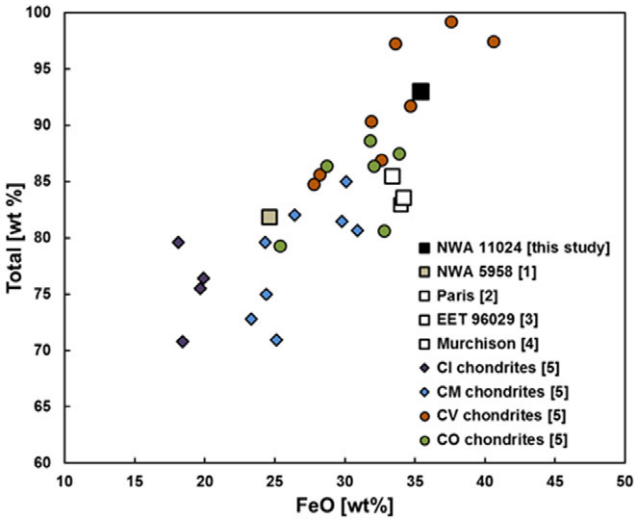

Fig. 19. FeO versus Total values of the matrix analyses in wt%. NWA 11024 has the highest FeO and total value of all known CM chondrites and is plotted within the CV field. [1] Jacquet et al. (2016); [2] Hewins et al. (2014); [3] Lee et al. (2016); [4] McSween and Richardson (1977); [5] McSween (1987). (Color figure can be viewed at wileyonlinelibrary.com.)

Magnetic properties measurements of NWA 11024 revealed a metal content of about ~1 vol% (2.1 wt%), which is similar to that of Paris but >5 times higher than for CM falls. However, point counting of the two thin sections of NWA 11024 shows a metal (+altered phases) content of ~2.5 vol%, which is somewhat higher. The reason for the discrepancy is terrestrial weathering, which destroyed a lot of metal and influenced the determination of the modal metal abundance. In detail, terrestrial weathering creates halos around the weathered metal grains, which let them appear larger than they really were. Furthermore, the magnetic susceptibility and saturation magnetization are affected by weathering of metal and provide a lower limit for the initial metal content. Despite this discrepancy, point counting and the magnetic measurements indicate an initial metal content of several wt% in NWA 11024, which can be interpreted as indication for a minor degree of aqueous alteration.

Additionally, it is assumed that a more-advanced alteration would result in a Fe depletion in the matrix (McSween 1979a, 1987). The matrix of NWA 11024 has a high FeO value and marks the upper end of CM chondrites together with those of the lower altered meteorites Murchison, Paris, and EET 96029 (Fig. 19). Likely caused by the heating process and the decomposition of hydrous minerals (also resulting in higher analytical totals of the matrix), NWA 11024 plots in the CV chondrite field and not together with the other less-altered CM chondrites.

In summary, the degree of aqueous alteration in NWA 11024 is lower than that considered for any other known CM chondrite (e.g., calcite grains and larger TCIs are missing). There is no doubt that water was present during the formation and evolution of the parent rock of NWA 11024 because small dehydrated former phyllosilicate patches (Fig. 8c) can be found in the matrix and in the fine-grained rims. However, it cannot completely be clarified if (1) there was only a minor content of water causing a low degree of aqueous alteration or if (2) the heat increased faster than in other CM chondrites and the time window for aqueous alteration was too short in order to enable a higher degree of aqueous alteration and the mixing of the different O-isotopic reservoirs.

Different Stages of Accretion and Alteration

Important questions are when and where the aqueous alteration took place? Two different models are possible (1) the pre-accretionary model (Metzler et al. 1992; Bischoff 1998; Ciesla et al. 2003) and (2) the parent body alteration model (McSween 1979b, 1987; Tomeoka and Buseck 1985; Browning et al. 1996). The parent body alteration model describes a scenario in which unaltered material accreted, forming the CM parent body and in situ aqueous alteration occurred. The pre-accretionary model implements a mixing of different altered and unaltered materials to form the parent body on which (besides impact brecciation) no (or only very minor) subsequent aqueous alteration took place. This pre-accretionary model includes aqueous alteration in the solar nebula (e.g., Ciesla et al. 2003) or in loosely consolidated, precursor planetary bodies which were destroyed by collision resulting in a mixing of the altered with nonaltered material prior to formation of second-generation parent body(ies) (Metzler et al. 1992; Bischoff 1998). In the pre-accretionary model, fragments of different sizes, compositions, and degrees of alteration should coexist next to each other which can be clearly observed in Bischoff et al. (2017a). Thus, fragments of different alteration stages are present and mixed together with unaltered material and in consequence, "reactive" unaltered phases can coexist and have common boundaries to heavily altered phases. In the parent body alteration model, the alteration products should basically consist of similar phases having the same (at least a very similar) degree of alteration.

Three points speak against the parent body alteration model for the evolution of NWA 11024.

1. The UCLIs were not formed as secondary products during aqueous alteration in the FGRs. They were formed at an earlier stage, within a different environment, and were subsequently mixed together with the unaltered material forming the FGR. A possible origin for the UCLIs is dust from an icy object like a loosely formed ice-rich parent body described by Metzler et al. (1992). The former phyllosilicates in the UCLIs decomposed to Fa-rich olivine and troilite by a heating event on the NWA 11024 parent body.
2. TCI pseudomorphs as shown in Fig. 8 are more likely clasts than in situ generated objects. Especially TCI-2 (Fig. 8b) has a FGR rim without UCLIs and a small AOA "sticking" onto the clast. If the FGRs are seen as accretionary dust mantels, then the TCI-2 patch cannot be formed by aqueous alteration on the parent body of NWA 11024.
3. TCI-1 has different patches of former TCI-clumps, which stick together. If they formed in situ, the different patches should have experienced the same conditions and consequently showing similar degree of aqueous alteration. However, the FeO/SiO_2 ratios vary significantly between the different patches, resulting in aqueous alteration indices (after Rubin et al. 2007) ranging from 2.2 to 2.8, which indicates different degrees of aqueous alteration. Furthermore, they strongly differ from TCI-2, which has a FeO/SiO_2 ratio of $\sim$1.0.

It is possible that additionally a mild aqueous alteration may have occurred on the final parent body resulting in the formation of small TCI-patches in the rims and the alteration of the chondrule mesostasis. But this alteration cannot explain mineralogical characteristics of the two large TCI-patches or the UCLIs within the FGRs. Consequently, pre-accretionary altered and unaltered material were accreted and NWA 11024 originated from a second-generation parent body.

CM-an or the First Type 3 CM Chondrite

The study has shown that only a minor degree of aqueous alteration occurred in the NWA 11024 parent body and that the sample is free of water-bearing minerals. NWA 11024 manifests the problem with the current classification scheme: It is difficult to classify CM chondrites, which have been aqueously altered, and then heated and dehydrated. In the actual classification scheme, type 2 chondrites are water-bearing chondrites, whereas type 3 chondrites are water-free (<1 wt%). This raises two questions as follows.

1. Can a dehydrated type 2 CM chondrite be regarded as a type 3 CM chondrite as it is assumed for e.g., the CV3 chondrite Allende (e.g., Krot et al. 2006)?

2. Is it possible to create a meteorite in the CM region without water? If a dehydrated type 2 CM chondrite cannot be regarded as a type 3 CM chondrite (see option [1]), is it then even possible that a type 3 CM chondrite can exist?

Considering the first question, it is known that CV chondrites have undergone alteration that resulted in the formation of secondary minerals like ferrous olivine (e.g., Krot et al. 1995, 1997b, 2004, 2006; Kojima and Tomeoka 1996). This alteration process created ferrous olivine ($Fa_{40–60}$; CV_{oxA}) but also nearly pure fayalite ($Fa_{90–100}$; CV_{oxB}) in CV chondrites (Krot et al. 2006). The altered TCI-patches in NWA 11024 show olivines up to Fa_{90} which is similar to the CV samples. This leads to the assumption that aqueous alteration and dehydration by thermal processes occurred in CV chondrites and in NWA 11024 resulting in recrystallization of ferrous olivine from phyllosilicates and dehydration of the meteorites. If this is really the case for, e.g., Allende, then either Allende has to be classified as a CV-an or NWA 11024 has to be classified as a CM3 chondrite.

If NWA 11024 cannot be a type 3 CM then the existence of CM3 chondrites is questionable. Water was widespread in the CM-forming region and CM chondrites experienced various and extensive degrees of aqueous alteration resulting in a high variability of alteration phases like different phyllosilicates and calcites. NWA 11024 shows a similar bulk composition to other CM chondrites and should have sampled a similar region of the solar nebula (Chizmadia and Brearley 2004). Therefore, ice and water must always have been present in the forming region of CM chondrite parent body(ies). It seems unlikely to create a CM chondrite completely without water but with similar oxygen isotope and bulk compositions compared with other CM chondrites. The only way to have a CM chondrite without water is if thermal dehydration after its formation is considered. Consequently, a type 3 CM chondrite has to be a dehydrated CM2 chondrite; otherwise it is questionable if a type 3 CM chondrite can exist.

CONCLUSION

The meteorite NWA 11024 is a unique sample of the CM parent body(ies) accretion region. The composition, mineralogical characteristics, as well as the oxygen isotopic data indicate strong similarities to other CM chondrites. However, unlike known CM chondrites, the effects of aqueous alteration in NWA 11024 are minimal and did not play a key role in the history. Calcite grains are missing, which are ubiquitous in even the least altered CM chondrites like Maribo or Paris and NWA 11024 is the CM chondrite affected by the lowest degree of aqueous alteration. A secondary heating event occurred and dehydrated the sample. This triggered the decomposition of phyllosilicates and formation of olivine and also increased the mean totals of the matrix to the highest known values for CM chondrites. Furthermore, the fine-grained rims contain small unknown clot-like inclusions (UCLIs). They are more S-rich than the surrounding rim and mixing of different material from different regions of solar nebula must have occurred. The compositions and mineralogy of the UCLIs are similar to those of cometary IDPs and a possible source is loosely consolidated first-generation planetesimals. Furthermore, the two larger TCI pseudomorphs are fragments showing that the sample NWA 11024 originates from a second-generation parent body. The current classification schemes cannot classify a CM chondrite with such a low degree of aqueous alteration, followed by a heating event. However, the missing of phyllosilicates and calcite grains and the dehydration of the NWA 11024 strongly speaks for a classification as a type 3 CM chondrite consistent with a CV3 classification, for, e.g., Allende.

Acknowledgments—The authors thank Knut Metzler and Markus Patzek for fruitful discussions. We thank Ulla Heitmann for sample preparation and Dr. Jasper Berndt-Gerdes and Beate Schmitte for analytical assistance. We acknowledge Sigrid Wengert (Osnabrück) and Sergey Vasilev (Prague) for contributing the sample and Fig. 1. We also appreciate the support and comments by Associate Editor Kevin Righter as well as the very helpful comments and suggestions by two anonymous reviewers. The SEM-FIB-TEM facility at the Universität Jena is funded by the DFG (grant LA 830/14-1); F. Langenhorst and FSU Jena (DRM/2016-01) are thanked for support of the work conducted at the facility. This work was also partly supported by the SFB-TRR 170 "Late Accretion onto Terrestrial Planets" (subproject B5). This is TRR 170 publication No. 44.

Editorial Handling—Dr. Kevin Righter

REFERENCES

Akai J. 1988. Incompletely transformed serpentine-type phyllosilicates in the matrix of Antarctic CM chondrites. *Geochimica et Cosmochimica Acta* 52:1593–1599.

Akai J. 1989. Mineralogical evidence of heating events in carbonaceous chondrites, Y-82621 and Y-86720. *Proceedings of the NIPR Symposium on Antarctic Meteorites* 14:22–23.

Akai J. 1990a. Mineralogical evidence of heating events in Antarctic carbonaceous chondrites, Y-86720 and Y-82162.

Proceedings of the NIPR Symposium on Antarctic Meteorites 3:55–68.

Akai J. 1990b. Thermal metamorphism in four Antarctic carbonaceous chondrites and its temperature scale estimated by T-T-T diagram. *Proceedings of the NIPR Symposium on Antarctic Meteorites* 15:86–87.

Akai J. 1992. TTT-diagram of serpentine and saponite, and estimation of metamorphic heating degree of Antarctic carbonaceous chondrites. *Proceedings of the NIPR Symposium on Antarctic Meteorites* 5:120–135.

Akai J. and Tari S. 1997. *Thermally metamorphosed Antarctic CM and CI carbonaceous chondrites in Japanese collections, and transformation processes of phyllosilicate*. LPI Technical Report 97-02, Part I. Houston, Texas: Lunar and Planetary Institute. pp. 1–2.

Alexander C. M. O'D., Bowden R., Fogel M. L., Howard K. T., Herd C. D. K., and Nittler L. R. 2012. The provenances of asteroids, and their contributions to the volatile inventories of the terrestrial planets. *Science* 337:721–723.

Alexander C. M. O'D., Howard K. T., Bowden R., and Fogel M. L. 2013. The classification of CM and CR chondrites using bulk H, C and N abundances and isotopic compositions. *Geochimica et Cosmochimica Acta* 123:244–260.

Anders E. and Grevesse N. 1989. Abundances of the elements: Meteoritic and solar. *Geochimica et Cosmochimica Acta* 53:197–214.

Armstrong J. T. 1991. Quantitative elemental analysis of individual microparticles with electron beam instruments. In *Electron probe quantitation*, edited by Heinrich K. F. J. and Newbury D. E. New York: Plenum Press. pp. 261–315.

Barrat J. A., Yamaguchi A., Greenwood R. C., Bohn M., Cotton J., Benoit M., and Franchi I. A. 2007. The Stannern trend eucrites: Contamination of Main-Group eucritic magmas by crustal partial melts. *Geochimica et Cosmochimica Acta* 71:4108–4124.

Barrat J. A., Yamaguchi A., Benoit M., Cotten J., and Bohn M. 2008. Geochemistry of diogenites: Still more diversity in their parental melts. *Meteoritics & Planetary Science* 43:1759–1775.

Barrat J.-A., Zanda B., Moynier F., Bollinger C., Liorzou C., and Bayron G. 2012. Geochemistry of CI chondrites: Major and trace elements, and Cu and Zn isotopes. *Geochimica et Cosmochimica Acta* 83:79–92.

Barrat J.-A., Dauphas N., Gillet P., Bollinger C., Etoubleau J., Bischoff A., and Yamaguchi A. 2016. Evidence from Tm anomalies for non-CI refractory lithophile element proportions in terrestrial planets and achondrites. *Geochimica et Cosmochimica Acta* 176:1–17.

Beyssac O., Goffé B., Chopin C., and Rouzad J. N. 2002. Raman spectra of carbonaceous material in metasediments: A new geothermometer. *Journal of Metamorphic Geology* 20:859–871.

Bischoff A. 1998. Aqueous alteration of carbonaceous chondrites: Evidence for preaccretionary alteration—A review. *Meteoritics & Planetary Science* 33:1113–1122.

Bischoff A. and Keil K. 1983. Ca-Al-rich chondrules and inclusions in ordinary chondrites. *Nature* 303:588–592.

Bischoff A. and Keil K. 1984. Al rich objects in ordinary chondrites: Related origin of carbonaceous and ordinary chondrites and their constituents. *Geochimica et Cosmochimica Acta* 48:693–709.

Bischoff A. and Metzler K. 1991. Mineralogy and petrography of the anomalous carbonaceous chondrites Yamato-86720, Yamato-82162, and Belgica-7904. *Proceedings of the NIPR Symposium on Antarctic Meteorites* 4:226–246.

Bischoff A. and Stöffler D. 1992. Shock metamorphism as a fundamental process in the evolution of planetary bodies: Information from meteorites. *European Journal of Mineralogy* 4:707–755.

Bischoff A., Scott E. R. D., Metzler K., and Goodrich C. A. 2006. Nature and origins of meteoritic breccias. In *Meteorites and the early solar system II*, edited by Lauretta D. S. and McSween H. Y. Jr. Tucson, Arizona: The University of Arizona Press. pp. 679–712.

Bischoff A., Ebert S., Metzler K., and Lentfort S. 2017a. Breccia classification of CM chondrites (abstract #6089). *Meteoritics & Planetary Science* 52:A26.

Bischoff A., Wurm G., Chaussidon M., Horstmann M., Metzler K., Weyrauch M., and Weinauer J. 2017b. The Allende multi-compound chondrule (ACC)—Chondrule formation in a local super-dense region of the early solar system. *Meteoritics & Planetary Science* 52:906–924.

Bland P. A., Zolensky M. E., Benedix G. K., and Sephton M. A. 2006. Weathering of chondritic meteorites. In *Meteorites and the early solar system II*, edited by Lauretta D. S. and McSween H. Y. Jr. Tucson, Arizona: The University of Arizona Press. pp. 853–867.

Bradley J. P. 1988. Analysis of chondritic interplanetary dust thin-sections. *Geochimica et Cosmochimica Acta* 52:889–900.

Bradley J. P. 1994. Chemically anomalous, preaccretionally irradiated grains in interplanetary dust from comets. *Science* 265:925–929.

Brearley A. J. 2006. The action of water. In *Meteorites and the early solar system II*, edited by Lauretta D. S. and McSween H. Y. Jr. Tucson, Arizona: The University of Arizona Press. pp. 587–624.

Brearley A. J. and Jones R. H. 1998. Chondritic meteorites. In *Planetary materials*, edited by Papike J. J. Reviews in Mineralogy, vol. 36. Washington, D.C.: Mineralogical Society of America. pp. 3-1–3-398.

Browning L. B., McSween H. Y. Jr., and Zolensky M. E. 1996. Correlated alteration effects in CM carbonaceous chondrites. *Geochimica et Cosmochimica Acta* 60:2621–2633.

Busemann H., Alexander C. M. O'D., and Nittler L. R. 2007. Characterization of insoluble organic matter in primitive meteorites by micro Raman spectroscopy. *Meteoritics & Planetary Science* 42:1387–1416.

Chizmadia L. J. 2005. Fine-grained rims of Y-791198 are texturally, mineralogically and compositionally similar to GEMS-type IDPs (abstract #2229). 36th Lunar and Planetary Science Conference. CD-ROM.

Chizmadia L. J. and Brearley A. J. 2004. Aqueous alteration of carbonaceous chondrites: New insights from comparative studies of two unbrecciated CM2, Y-971198 and ALH81002 (abstract #1419). 35th Lunar and Planetary Science Conference. CD-ROM.

Chizmadia L. J. and Brearley A. J. 2008. Mineralogy, aqueous alteration, and primitive textural characteristics of fine-grained rims in the Y-791198 CM2 carbonaceous chondrite: TEM observations and comparison to ALHA81002. *Geochimica et Cosmochimica Acta* 72:602–625.

Ciesla F. and Lauretta D. 2005. Radial migration and dehydration of phyllosilicates in the solar nebula. *Earth and Planetary Science Letters* 231:1–8.

Ciesla F. J., Lauretta D. S., Cohen B. A., and Hood L. L. 2003. A nebular origin for chondritic fine-grained phyllosilicates. *Science* 299:549–552.

Clayton R. N. and Mayeda T. K. 1984. The oxygen isotope record in Murchison and other carbonaceous chondrites. *Earth and Planetary Science Letters* 67:151–161.

Clayton R. N. and Mayeda T. K. 1999. Oxygen isotope studies of carbonaceous chondrites. *Geochimica et Cosmochimica Acta* 63:2089–2104.

Cotten J., Ledez A., Bau M., Caroff M., Maury R. C., Dulski P., Fourcade S., Bohn M., and Brousse R. 1995. Origin of anomalous rare-earth element and yttrium enrichments in subaerially exposed basalts—Evidence from French-Polynesia. *Chemical Geology* 119:115–138.

Cournede C., Gattacceca J., Gounelle M., Rochette P., Weiss B. P., and Zanda B. 2015. An early solar system magnetic field recorded in CM chondrites. *Earth and Planetary Science Letter* 410:62–74.

Deer W. A., Howie R. A., and Zussmann J. 1992. *An introduction to the rock-forming minerals*, 2nd ed. Essex, UK: Longman Scientific and Technical.

De Leuw S., Rubin A. E., Schmitt A. K., and Wasson J. T. 2009. ^{53}Mn-^{53}Cr systematics of carbonates in CM chondrites: Implications for the timing and duration of aqueous alteration. *Geochimica et Cosmochimica Acta* 73:7433–7442.

Dodd R. T. 1981. *Meteorites—A petrologic-chemical synthesis*. Cambridge, UK: Cambridge University Press. 376 p.

Dyl K. A., Bischoff A., Ziegler K., Young E. D., Wimmer K., and Bland P. A. 2012. Early solar system hydrothermal activity in chondritic asteroids on 1-10-year timescales. *Proceedings of the National Academy of Sciences* 109:18,306–18,311.

Ebert S. and Bischoff A. 2015. Formation of Na-rich chondrules by melting of Na-rich and condensed (ultra)-refractory precursors (abstract #5062). *Meteoritics & Planetary Science* 50:A89.

Ebert S. and Bischoff A. 2016. Genetic relationship between Na-rich chondrules and Ca, Al-rich inclusions? Formation of Na-rich chondrules by melting of refractory and volatile precursors in the solar nebula. *Geochimica et Cosmochimica Acta* 177:182–204.

Ebert S., Bischoff A., Harries D., Barrat J.-A., Pack A., Lentfort S., Kimpel S., Vasilev S., and Wengert S. 2017a. Northwest Africa 11024—The first CM3 chondrite or a dehydrated anomalous carbonaceous chondrite? (abstract #1903). 48th Lunar and Planetary Science Conference. CD-ROM.

Ebert S., Render J., Brennecka G. A., Burkhardt C., Bischoff A., and Kleine T. 2017b. ^{50}Ti evidence for different refractory precursors in chondrules (abstract #6255). *Meteoritics & Planetary Science* 52:A79.

Ebert S., Render J., Brennecka G. A., Burkhardt C., Bischoff A., Gerber S., and Kleine T. 2018. Ti isotopic evidence for a non-CAI refractory component in the inner solar system. *Earth and Planetary Science Letters* 498:257–265.

Endreß M. and Bischoff A. 1996. Carbonates in CI chondrites. Clues to parent body evolution. *Geochimica et Cosmochimica Acta* 60:489–507.

Endreß M., Keil K., Bischoff A., Spettel B., Clayton R. N., and Mayeda T. K. 1994. Origin of dark clasts in the Acfer 059/El Djouf 001 CR2 chondrite. *Meteoritics* 29:26–40.

Endress M., Zinner E., and Bischoff A. 1996. Early aqueous activity on primary meteorite parent bodies. *Nature* 379:701–703.

Fioretti A. M., Goodrich C. A., Shaddad M., Jenniskens P., Zolensky M., Kohl I., Young E., Rumble D., Kita N., Turrin B., and Herzog G. 2017. A report on 63 newly sampled stones of the Almahata Sitta fall (Asteroid 2008 TC3) from the University of Khartoum Collection, including a C2 carbonaceous chondrite (abstract #1419). 48th Lunar and Planetary Science Conference. CD-ROM.

Fraundorf P. 1981. Interplanetary dust in the transmission electron microscope: Diverse materials from the early solar system. *Geochimica et Cosmochimica Acta* 45:915–943.

Fuchs L. H., Olsen E., and Jensen K. J. 1973. Mineralogy, mineral-chemistry, and composition of the Murchison (C2) meteorite. *Smithsonian Contribution to the Earth Sciences* 10:1–39.

Fujiya W., Sugiura N., Hotta H., Ichimura K., and Sano Y. 2012. Evidence for the late formation of hydrous asteroids from young meteoritic carbonates. *Nature Communications* 3:627.

Gaffey M. J., Burbine T. H., and Binzel R. P. 1993. Asteroid spectroscopy: Progress and perspectives. *Meteoritics* 28:161–187.

Gail H.-P., Trieloff M., Breuer D., and Spohn T. 2014. Early thermal evolution of planetesimals and its impact on processing and dating of meteoritic material. In *Protostars and planets VI*, edited by Beuther H., Klessen R., Dullemond C., and Henning T. Tucson, Arizona: The University of Arizona Press. pp. 571–593.

Garenne A., Beck P., Montes-Hernandez G., Chiriac R., Toche F., Quirico E., Bonal L., and Schmitt B. 2014. The abundance and stability of "water" in type 1 and 2 carbonaceous chondrites (CI, CM and CR). *Geochimica et Cosmochimica Acta* 137:93–112.

Gattacceca J., Suavet C., Rochette P., Weiss B. P., Winklhofer M., Uehara M., and Friedrich J. M. 2014. Metal phases in ordinary chondrites: Magnetic hysteresis properties and implications for thermal history. *Meteoritics & Planetary Science* 49:652–676.

Gattacceca J., Weiss B. P., and Gounelle M. 2016. New constraints on the magnetic history of the CV parent body and the solar nebula from the Kaba meteorite. *Earth and Planetary Science Letter* 455:166–175.

Gooding J. L. and Zolensky M. E. 1987. Thermal stability of tochilinite. Proceedings, 18th Lunar and Planetary Science Conference. pp. 343–344.

Greenwood C. A., Franchi I. A., Kearsley A. T., and Alard O. 2010. The relationship between CK and CV chondrites. *Geochimica et Cosmochimica Acta* 74:1684–1705.

Grimm R. E. and McSween H. Y. Jr. 1989. Water and the thermal evolution of carbonaceous chondrite parent bodies. *Icarus* 82:244–280.

Grossman L. and Larimer J. W. 1974. Early chemical history of the solar system. *Review of Geophysics and Space Physics* 12:71–101.

Haack H., Grau T., Bischoff A., Horstmann M., Wasson J., Sørensen A., Laubenstein M., Ott U., Palme H., Gellissen M., Greenwood R. C., Pearson V. K., Franchi I. A., Gabelica Z., and Schmitt-Kopplin P. 2012. Maribo—A new CM fall from Denmark. *Meteoritics & Planetary Science* 47:30–50.

Harries D. and Langenhorst F. 2013. The nanoscale mineralogy of Fe, Ni sulfides in pristine and metamorphosed CM and CM/CI-like chondrites: Tapping

a petrogenetic record. *Meteoritics & Planetary Science* 48:879–903.

Hewins R. H., Bourot-Denise M., Zanda B., Leroux H., Barrat J.-A., Humayun M., Göpel C., Greenwood R. C., Franchi I. A., Pont S., Lorand J.-P., Cournède C., Gattacceca J., Rochette P., Kuga M., Marrocchi Y., and Marty B. 2014. The Paris meteorite, the least altered CM chondrite so far. *Geochimica et Cosmochimica Acta* 124:190–222.

Hillert M. and Qiu C. 1991. A thermodynamic assessment of the Fe-Cr-Ni-C system. *Metallurgical and Material Transaction A* 22:2187–2198.

Hiroi T. and Zolensky M. E. 1999. UV-VIS-NIR absorption features of heated phyllosilicates as remote-sensing clues of thermal histories of primitive asteroids. *Proceedings of the NIPR Symposium on Antarctic Meteorites* 12:108–116.

Hiroi T., Pieters C. M., Zolensky M. E., and Lipschutz M. E. 1993. Evidence of thermal metamorphism of C, G, B, and F asteroid. *Science* 261:1016–1018.

Hiroi T., Pieters C. M., Zolensky M. E., and Lipschutz M. E. 1994. Possible thermal metamorphism of the C, G, B, and F asteroids detected from their reflectance spectra in comparison with carbonaceous chondrites. *Proceedings of the NIPR Symposium on Antarctic Meteorites* 7:230–243.

Hiroi T., Pieters C. M., Zolensky M. E., and Lipschutz M. P. 1996. Thermal metamorphism of the C, G, B and F asteroids seen from the 0.7 μm, 0.3 μm, and UV absorption strengths in comparison with carbonaceous chondrites. *Meteoritics & Planetary Science* 31:321–327.

Homma Y., Kouketsu Y., Kagi H., Mikouchi T., and Yabuta H. 2015. Raman spectroscopic thermometry of carbonaceous material in chondrites: Four–band fitting analysis and expansion of lower temperature limit. *Journal of Mineralogical and Petrological Sciences* 110:276–282.

Howard K. T., Benedix G. K., Bland P. A., and Cressey G. 2009. Modal mineralogy of CM2 chondrites by X-ray diffraction (PSD-XRD). Part 1: Total phyllosilicate abundance and the degree of aqueous alteration. *Geochimica et Cosmochimica Acta* 73:4576–4589.

Ikeda Y. 1992. An overview of the research consortium, "Antarctic carbonaceous chondrites with CI affinities, Yamato-86720, Yamato-82162, and Belgica-7904." *Proceedings of the NIPR Symposium on Antarctic Meteorites* 5:49–73.

Irmer G. 1985. Zum Einfluss der Apparatfunktion auf die Bestimmung vom Streuquerschnitt und Lebensdauern aus optischen Phononenspektren. *Experimentelle Technik der Physik* 33:501–506.

Jacquet E., Barrat J.-A., Beck P., Caste F., Gattacceca J., Sonzogni C., and Gounelle M. 2016. Northwest Africa 5958: A weakly altered CM-related ungrouped chondrite, not a CI3. *Meteoritics & Planetary Science* 51:851–869.

Jarosewich E. 1990. Chemical analyses of meteorites: A compilation of stony and iron meteorite analyses. *Meteoritics* 25:323–337.

Kallemeyn G. W. and Wasson T. J. 1981. The compositional composition of chondrites—I. The carbonaceous chondrite groups. *Geochimica et Cosmochimica Acta* 45:1217–1230.

Kallemeyn G. W. and Wasson T. J. 1982. The compositional composition of chondrites: III. Ungrouped carbonaceous chondrites. *Geochimica et Cosmochimica Acta* 46:2217–2228.

Kallemeyn G. W., Rubin A. E., and Wasson T. J. 1994. The compositional composition of chondrites: VI. The CR carbonaceous chondrite group. *Geochimica et Cosmochimica Acta* 58:2873–2888.

Kallemeyn G. W., Rubin A. E., and Wasson T. J. 1996. The compositional composition of chondrites: VII. The R chondrite group. *Geochimica et Cosmochimica Acta* 60:2243–2256.

Kanno A., Hiroi T., Nakamura R., Abe M., Ishiguro M., Hasegawa S., Miyasaka S., Sekiguchi T., Terada H., and Igarashi G. 2003. The first detection of water absorption on a D type asteroid. *Geophysical Research Letters* 30:1909–1913.

Kerridge J. F. and Bunch T. E. 1979. Aqueous activity on asteroids: Evidence from carbonaceous chondrites. In *Asteroids*, edited by Gehrels T. Tucson, Arizona: The University of Arizona Press. pp. 745–764.

Kimura M., Grossman J. N., and Weisberg M. K. 2011. Fe-Ni metal and sulfide minerals in CM chondrites: An indicator for thermal history. *Meteoritics & Planetary Science* 46:431–442.

Kojima T. and Tomeoka K. 1996. Indicators of aqueous alteration and thermal metamorphism on the CV3 parent body: Microtextures of a dark inclusions from Allende. *Geochimica et Cosmochimica Acta* 60:2651–2666.

Kouketsu Y., Mizukami T., Mori H., Endo S., Aoya M., Hara H., Nakamura D., and Wallis S. 2014. A new approach to develop the Raman carbonaceous material geothermometer for low-grade metamorphism using peak width. *Island Arc* 23:33–50.

Krot A. N., Scott E. R. D., and Zolensky M. E. 1995. Mineralogic and chemical variations among CV3 chondrites and their components: Nebular and asteroidal processing? *Meteoritics* 30:748–775.

Krot A. N., Rubin A. E., Keil K., and Wasson J. T. 1997a. Microchondrules in ordinary chondrites: Implications for chondrule formation. *Geochimica et Cosmochimica Acta* 61:463–473.

Krot A. N., Scott E. R. D., and Zolensky M. E. 1997b. Origin of fayalitic olivine rims and plate-like matrix olivine in the CV3 chondrite Allende and its dark inclusions. *Meteoritics* 32:31–49.

Krot A. N., Petaev M. I., and Bland P. A. 2004. Multiple formation mechanisms olivine in CV carbonaceous chondrites during fluid-assisted metamorphism. *Antarctic Meteorite Research* 17:153–171.

Krot A. N., Hutcheon I. D., Brearley A. J., Pravdivtseva O. V., Petaev M. I, and Hohenberg C. M. 2006. Timescales and settings for alteration of chondritic meteorites. In *Meteorites and the early solar system II*, edited by Lauretta D. S. and McSween H. Y. Jr. Tucson, Arizona: The University of Arizona Press. pp. 525–553.

Lee M. R., Lindgren P., King A. J., Greenwood R. C., Franchi I. A., and Sparkes R. 2016. Elephant Moraine 96029, a very mildly aqueously and heated carbonaceous chondrite: Implications for the drivers of parent body processes. *Geochimica et Cosmochimica Acta* 187:237–259.

Lindgren P., Lee M. R., Sofe M. R., and Zolensky M. E. 2013. Clasts in the CM2 carbonaceous chondrite Lonewolf Nunataks 94101: Evidence for aqueous alteration prior to complex mixing. *Meteoritics & Planetary Science* 48:1074–1090.

Lipschutz M. E., Zolensky M. E., and Bell M. S. 1999. New petrographic and trace element data on thermally metamorphosed carbonaceous chondrites. *Antarctic Meteorite Research* 12:57–80.

Lodders K. and Fegley B. Jr. 1998. *The planetary scientist's companion*. New York: Oxford University Press. 371 p.

Lodders K., Palme H., and Gail H. P. 2009. Abundances of the elements in the solar system. In *Landolt-Börnstein, New Series, Vol. VI/4B*, edited by Trümper J. E. Berlin, Heidelberg: Springer-Verlag. pp. 560–630.

MacPherson G. J. 2014. Calcium-aluminum-rich inclusions in chondritic meteorites. In *Treaties on geochemistry*, vol. 2, edited by Davis A. M., Holland H. D., and Turekian K. K. Amsterdam, the Netherlands: Elsevier. pp. 139–179.

Marrocci Y., Gounelle M., Blanchard I., Caste F., and Kearsley A. T. 2014. The Paris CM chondrite: Secondary minerals and asteroidal processing. *Meteoritics & Planetary Science* 49:1232–1249.

Mayeda K. and Clayton R. N. 1990. Oxygen isotopic compositions of B-7904, Y-82162, and Y-86720. *Proceedings of the NIPR Symposium on Antarctic Meteorites* 15:196–197.

Mayeda K., Clayton R. N., and Yanai K. 1987. Oxygen isotopic compositions of several Antarctic meteorites. *Proceedings of the 46th Symposium on Antarctic Meteorites*. pp. 144–150.

McSween H. Y. Jr. 1977. Chemical and petrological constraints on the origin of chondrules and inclusions in carbonaceous chondrites. *Geochimica et Cosmochimica Acta* 41:1843–1860.

McSween H. Y. Jr. 1979a. Alteration in CM carbonaceous chondrites inferred from modal and chemical variations in matrix. *Geochimica et Cosmochimica Acta* 43:1761–1770.

McSween H. Y. Jr. 1979b. Are carbonaceous chondrites primitive or processed? *Reviews of Geophysics and Space Physics* 17:1059–1078.

McSween H. Y. Jr. 1987. Aqueous alteration in carbonaceous chondrites: Mass balance constraints on matrix mineralogy. *Geochimica et Cosmochimica Acta* 51:2469–2477.

McSween H. Y. Jr. and Richardson S. M. 1977. The composition of carbonaceous chondrite matrix. *Geochimica et Cosmochimica Acta* 41:1145–1161.

McSween H. Y. Jr., Sears D. W. G., and Dodd R. T. 1988. Thermal metamorphism. In *Meteorites and the early solar system*, edited by Kerridge J. F. and Matthews M. S. Tucson, Arizona: The University of Arizona Press. pp. 102–113.

Metzler K. 1995. Aqueous alteration of primary rock on the CM parent body. Proceedings, 26th Lunar and Planetary Science Conference. pp. 961–962.

Metzler K. 2004. Formation of accretionary dust mantles in the solar nebula: Evidence from preirradiated olivines in CM chondrites. *Meteoritics & Planetary Science* 39:1307–1319.

Metzler K. and Bischoff A. 1996. Constraints on chondrites agglomeration from fine-grained chondrule rims. In *Chondrules and the protoplanetary disk*, edited by Hewins R. H., Jones R. H., and Scott E. R. D. Cambridge, UK: Cambridge University Press. pp. 153–161.

Metzler K., Bischoff A., and Stöffler D. 1992. Accretionary dust mantles in CM chondrites: Evidence for solar nebula processes. *Geochimica et Cosmochimica Acta* 56:2873–2897.

Michel P. and Delbo M. 2010. Orbital and thermal evolutions of four potential targets for a sample return space mission to a primitive near-Earth asteroid. *Icarus* 209:520–534.

Morlok A., Bischoff A., Stephan T., Floss C., Zinner E. K., and Jessberger E. K. 2006. Brecciation and chemical heterogeneities of CI chondrites. *Geochimica et Cosmochimica Acta* 70:5371–5394.

Nakamura T. 2005. Post-hydration thermal metamorphism of carbonaceous chondrites. *Journal of Mineralogical and Petrological Science* 100:260–272.

Nakamura T. 2006. Yamato 793321 CM chondrite: Dehydrated regolith material of a hydrous asteroid. *Earth and Planetary Science Letters* 242:26–38.

Nakato A., Nakamura T., Kitajima F., and Noguchi T. 2008. Evaluation of dehydration mechanism during heating of hydrous asteroids based on mineralogical and chemical analysis of naturally and experimentally heated CM chondrites. *Earth, Planets and Space* 60:855–864.

Pack A., Tanaka R., Hering M., Sengupta S., Peters S., and Nakamura E. 2016. The oxygen isotope composition of San Carlos olivine on VSMOW2-SLAP2 scale. *Rapid Communications of Mass Spectrometry* 30:1495–1504.

Palme H. and Jones A. 2003. Solar system abundances of the elements. In *Meteorites, comets, and planets*, edited by Davis A. M. Treatise on Geochemistry, vol. 1. Oxford, UK: Elsevier. pp. 41–63.

Patzek M. and Bischoff A. 2015. Search and characterization of volatile-rich clasts in brecciated meteorites (abstract #5057). *Meteoritics & Planetary Science* 50:A261.

Patzek M., Ebert S., and Bischoff A. 2016. New volatile-rich clasts from brecciated chondrites and achondrites (abstract #6136). *Meteoritics & Planetary Science* 51:A511.

Patzek M., Visser R., Bischoff A., and John T. 2018. Mineralogy of volatile-rich clasts in brecciated meteorites. *Meteoritics & Planetary Science*. https://doi.org/10.1111/maps.13175

Paul R. L. and Lipschutz M. E. 1990. Consortium study of labile trace elements in some Antarctic carbonaceous chondrites: Antarctic and non-Antarctic meteorite comparisons. *Proceedings of the NIPR Symposium on Antarctic Meteorites* 3:80–95.

Petaev M. I. and Wood J. A. 1998. The condensation with partial isolated (CWPI) model of condensation in the solar system. *Meteoritics & Planetary Science* 33:1123–1137.

Podosek F. A. and Cassen P. 1994. Theoretical, observational, and isotopic estimates of the lifetime of the solar nebula. *Meteoritics* 29:6–25.

Richardson S. M. 1978. Vein formation in the C1 carbonaceous chondrite. *Meteoritics* 13:141–159.

Rietmeijer F. J. M. 1998. Interplanetary dust particles. In *Planetary materials*, edited by Papike J. J. Reviews in Mineralogy, vol. 36. Washington, D.C.: Mineralogical Society of America. pp. 2-1–2-95.

Rivkin A. S., Campins H., Emery J. P., Howell E. S., Licandro J., Takir D., and Vilas F. 2015. Astronomical observations of volatiles on asteroids. In *Asteroids IV*, edited by Michel P., DeMeo F. E., and Bottke W. F. Tucson, Arizona: The University of Arizona Press. pp. 65–87.

Rubin A. E. 2011. Origin of the differences in refractory-lithophile-element abundances among chondrite groups. *Icarus* 213:547–558.

Rubin A. E. 2015. An American on Paris: Extent of aqueous alteration of a CM chondrite and the petrography of its refractory and amoeboid olivine inclusions. *Meteoritics & Planetary Science* 50:1595–1612.

Rubin A. E. and Wasson J. T. 1986. Chondrules in the Murray CM2 meteorite and compositional differences

between CM-CO and ordinary chondrite chondrules. *Geochimica et Cosmochimica Acta* 50:307–315.
Rubin A. E., Trigo-Rodríguez J. M., Huber H., and Wasson J. T. 2007. Progressive aqueous alteration of CM carbonaceous chondrites. *Geochimica et Cosmochimica Acta* 71:2361–2382.
Scott E. R. D., Keil K., and Stöffler D. 1992. Shock metamorphism of carbonaceous chondrites. *Geochimica et Cosmochimica Acta* 56:4281–4293.
Sephton M. A. 2004. Organic matter in ancient meteorites. *Astronomy & Geophysics* 45:2.8–2.14.
Sharp Z. D. 1990. A laser-based microanalytical technique for in situ determination of oxygen isotope ratios of silicates and oxides. *Geochimica et Cosmochimica Acta* 54:1353–1357.
Shoemaker E. M. 1977. Why study impact craters. In *Impact and explosions cratering*, edited by Roddy D. J., Pepin R. O., and Merrill R. B. New York: Pergamon Press. pp. 1–10.
Stelzner T., Heide K., Bischoff A., Weber D., Scherer P., Schultz L., Happel M., Schrön W., Neupert U., Michel R., Clayton R. N., Mayeda T. K., Bonani G., Haidas I., Ivy-Ochs S., and Sutter M. 1999. An interdisciplinary study of weathering effects in ordinary chondrites from the Acfer region, Algeria. *Meteoritics & Planetary Science* 34:787–794.
Stöffler D., Keil K., and Scott E. R. D. 1991. Shock metamorphism of ordinary chondrites. *Geochimica et Cosmochimica Acta* 55:3845–3867.
Stöffler D., Hamann C., and Metzler K. 2018. Invited Review—Shock metamorphism of planetary silicate rocks and sediments: Proposal for an updated classification system. *Meteoritics & Planetary Science* 53:5–49.
Tomeoka K. 1989. Belgica-7904: A new kind of carbonaceous chondrite from Antarctica; mineralogy and petrology. *Proceedings of the NIPR Symposium on Antarctic Meteorites* 14:18–20.
Tomeoka K. and Buseck P. R. 1985. Indicators of aqueous alteration in CM carbonaceous chondrites: Microtextures of a layered mineral containing Fe, S, O, and Ni. *Geochimica et Cosmochimica Acta* 49:2149–2163.
Tomeoka K., Kojima H., and Yanai K. 1989. Yamato-86720: A CM carbonaceous chondrite having experienced extensive aqueous alteration and thermal metamorphism. *Proceedings of the NIPR Symposium on Antarctic Meteorites* 2:55–74.
Tonui E. K., Zolensky M. E., and Lipschutz M. E. 2002. Petrography, mineralogy and trace element chemistry of Yamato-86029, Yamato-793321 and Lewis Cliff 85332: Aqueous alteration and heating events. *Antarctic Meteorite Research* 15:38–58.
Tonui E. K., Zolensky M. E., Lipschutz M. E., Wang M., and Nakamura T. 2003. Yamato 86029: Aqueously altered and thermally metamorphosed CI chondrite with unusual textures. *Meteoritics & Planetary Science* 38:269–292.
Tonui E., Zolensky M., Hiroi T., Nakamura T., Lipschutz M. E., Wang M.-S., and Okudaira K. 2014. Petrographic, chemical and spectroscopic evidence for thermal metamorphism in carbonaceous chondrites I: CI and CM chondrites. *Geochimica et Cosmochimica Acta* 126:284–306.
Trigo-Rodríguez J. M., Rubin A. E., and Wasson J. A. 2006. Non-nebular origin of dark mantles around chondrules and inclusions in CM chondrites. *Geochimica et Cosmochimica Acta* 70:1271–1290.
Tyburczy J. A., Frisch B., and Ahrens T. J. 1986. Shock induced volatile loss from a carbonaceous chondrite: Implications for planetary accretion. *Earth and Planetary Science Letters* 80:201–207.
Van Cappellen E. and Doukhan J. C. 1994. Quantitative transmission X-ray microanalysis of ionic compounds. *Ultramicroscopy* 53:343–349.
Van Schmus W. R. and Wood J. A. 1967. A chemical-petrologic classification for the chondritic meteorites. *Geochimica et Cosmochimica Acta* 31:747–765.
Verdier-Paoletti M. J., Marrocchi Y., Avice G., Roskosz M., Gurenko A., and Gounelle M. 2017. Oxygen isotope constraints on the alteration temperatures of CM chondrites. *Earth and Planetary Science Letters* 458:273–281.
Vernazza P., Marsset M., Beck P., Binzel R. P., Birlan M., Cloutis E. A., DeMeo F. E., Dumas C., and Hiroi T. 2016. Compositional homogeneity of CM parent bodies. *The Astrophysical Journal* 152:54.
Vilas F. and Gaffey M. J. 1989. Phyllosilicates absorption features in main-belt and outer-belt asteroids from reflectance spectroscopy. *Science* 246:790–792.
Waldner P. and Pelton A. D. 2004. Thermodynamic assessment of the Fe-Ni-S system. *Metallurgical and Material Transaction B* 35:897–907.
Waldner P. and Pelton A. D. 2005. Thermodynamic modeling of the Fe-S system. *Journal of Phase Equilibria and Diffusion* 26:23–38.
Wang H., Weiss B. P., Bai X.-N., Downey B. G., Wang J., Wang J., Suavet C., Fu R. R., and Zucolotto M. E. 2017. Lifetime of the solar nebula constrained by meteorite paleomagnetism. *Science* 355:623–627.
Wasson J. T. and Trigo-Rodríguez J. M. 2004. Evaporation during chondrule, recondensation as fine particles, and the condensation of S and other volatile elements (abstract #2140). 35th Lunar and Planetary Science Conference. CD-ROM.
Wasson J. T., Krot A. N., Lee M. S., and Rubin A. E. 1995. Compound chondrules. *Geochimica et Cosmochimica Acta* 59:1847–1869.
Wlotzka F. 1993. A weathering scale for the ordinary chondrites. *Meteoritics* 28:460.
Zolensky M. E. and McSween H. Y. Jr. 1988. Aqueous alteration. In *Meteorites and the early solar system*, edited by Kerridge J. F., and Matthews M. S. Tucson, Arizona: The Univesity of Arizona Press. pp. 114–143.
Zolensky M. E., Bourcier W. L., and Gooding J. L. 1989a. Aqueous alteration on the hydrated asteroids: Results of EQ3/6 computer simulations. *Icarus* 78:411–425.
Zolensky M. E., Barrett R. A., and Prinz M. 1989b. Petrography, mineralogy and matrix compositions of Yamato-82162, a new CI2 chondrite. Proceedings, 20th Lunar and Planetary Science Conference. pp. 1253–1254.
Zolensky M. E., Prinz M., and Lipschutz M. 1991. Mineralogy and thermal history of Y-82162, Y-86720, and B-7904. *Proceedings of the NIPR Symposium on Antarctic Meteorites* 16:195–196.
Zolensky M. E., Barrett R., and Browning L. 1993. Mineralogy and composition of matrix and chondrule rims in carbonaceous chondrites. *Geochimica et Cosmochimica Acta* 57:2123–3148.

Zolensky M. E., Weisberg M. K., Buchanan P. C., and Mittlefehldt D. W. 1996. Mineralogy of carbonaceous chondrite clasts in HED achondrites and the Moon. *Meteoritics & Planetary Science* 31:518–537.

Zolensky M. E., Bodnar R. J., Gibson E. K., Nyquist L. E. Jr., Reese Y., Shih C.-Y., and Wiesmann H. 1999. Asteroidal water within fluid inclusions-bearing halite in an H5 chondrite, Monahans (1998). *Science* 185:1377–1379.

SUPPORTING INFORMATION

Additional supporting information may be found in the online version of this article:

Table S1. Representative compositions of olivine and pyroxene of NWA 11024 matrix.

Table S2. Representative compositions of 72 randomly set measurements points of NWA 11024 matrix.

Table S3. Representative compositions of 106 randomly set measurements points in fine-grained rims of NWA 11024.

Table S4. Representative compositions of 83 randomly set measurements points in unknown clot-like inclusions from NWA 11024.

Table S5. Representative compositions of various phases in Ca,Al-rich inclusions from NWA 11024.